28p

[redacted]

X63-12016-X63-12019

Code 24

UNCLASSIFIED

Quarterly Summary Report No. 38-10

for the period October 1, 1962 to December 31, 1962

CLASSIFICATION CHANGE
TO UNCLASSIFIED
By authority of E.O. 11652
Changed by L. SHIRLEY Date 5-25-73

[redacted]

jpl

JET PROPULSION LABORATORY
CALIFORNIA INSTITUTE OF TECHNOLOGY
PASADENA, CALIFORNIA

January 31, 1963

(JPL-QSR-38-10) QUARTERLY SUMMARY REPORT NO. 38-10 FOR THE PERIOD 1 OCTOBER - 31 DECEMBER 1962 (Jet Propulsion Lab.) 28 p

N73-74367
THRU
N73-74370
Unclas
00/99 19335

This document contains information affecting the national defense of the United States, within the meaning of the Espionage Laws, Title 18 U.S.C., Sections 793 and 794, the transmission or revelation of which in any manner to an unauthorized person is prohibited by law.

[redacted]

CONFIDENTIAL

NATIONAL AERONAUTICS AND SPACE ADMINISTRATION
CONTRACT NO. NAS 7-100

Quarterly Summary Report No. 38-10

for the period October 1, 1962 to December 31, 1962

Copy No. 0295

JET PROPULSION LABORATORY
CALIFORNIA INSTITUTE OF TECHNOLOGY
PASADENA, CALIFORNIA

January 31, 1963

CONFIDENTIAL
GROUP 4 Downgraded at 3 year intervals:
declassified after 12 years.

Preface

This report is a quarterly summary of the research activities conducted by the Jet Propulsion Laboratory in the field of nondestructive testing of solid-propellant rocket motors. Section I details the progress in specific areas of research. An introduction to the problems and objectives of the program is given in *QSR 38-1*; a bibliography of the subject is presented in *QSR 38-1*, *-2*, and *-3*; Section I of *QSR 38-4* presents a general description of the subject areas covered by the entire program.

The work reported herein is undertaken in partial fulfillment of the Advanced Research Projects Agency Letter Order No. 107-60, for the National Aeronautics and Space Administration.

W. H. Pickering

W. H. Pickering, *Director*
Jet Propulsion Laboratory

This document contains information affecting the national defense of the United States, within the meaning of the Espionage Laws, Title 18, U.S.C., Sections 793 and 794, the transmission or revelation of which in any manner to an unauthorized person is prohibited by law.

Quarterly Summary Report No. 38-10

Copyright © 1963
Jet Propulsion Laboratory
California Institute of Technology

Contents

I. Physical Properties Studies 1

A. Polymer Degradation Mechanisms, *J. D. Ingham and N. S. Rapp* 1 X63-12017

B. A Study of the Ultimate Properties of Amorphous Gum Vulcanizates, *R. F. Fedors and R. F. Landel* 4 X63-12018

C. Continuous Medium Theory Applied to Viscoelastic Strain Analysis, II, *A. San Miguel* 8 X63-12019

References 22

I. Physical Properties Studies

A. Polymer Degradation Mechanisms

J. D. Ingham and N. S. Rapp

1. Kinetic Studies of Chain Scission of POPG–TDI and a Block (POEG–POP)–TDI Polymer

Degradation of polymers is being studied to provide a chemical basis for the development of nondestructive test methods applicable to solid propellants which may undergo chemical changes before use. Thermal degradation of uncrosslinked polyoxypropylene glycol–toluene diisocyanate polymer (POPG–TDI) and related polymers are being investigated to determine the mechanism of bond scission.

Although chain scission of POPG–TDI at 200°C has been shown to take place predominately at the urethane bonds by a random mechanism (*SPS 37-17*, Vol. IV) it is not expected that all the urethane bonds will break at the same rate. The 2- or 4-isocyanate groups form bonds with primary or secondary hydroxyls of different stability and these four possible urethane types will degrade at different rates. Furthermore, weak links other than urethanes can be postulated, for example, peroxides in the polyether, or dimerized isocyanates. In an attempt to determine whether the initial rate of bond scission would be decreased by a larger concentration of primary hydroxyl groups in the starting polyoxyalkylene glycol, a block (polyoxyethylene glycol–polyoxypropylene)–toluene diisocyanate (POEG–POP)–TDI polymer was prepared for degradation. The POPG was reacted with sodium and then treated with ethylene oxide at 130 to 140°C until 3.76 mole of epoxide per equivalent of hydroxyl was reacted. After thorough washing and drying the POEG–POP was reacted with TDI. A similar polyurethane was prepared from unmodified POPG and both samples were degraded at 200°C under helium. The degradation was followed by withdrawing samples for intrinsic viscosity $[\eta]$, and infrared measurements. Although the infrared studies indicated decreasing urethane hydrogen and increasing hydroxyl at large extents of degradation, because of band overlap and sample and cell variability, quantitative results were not obtained. From η the weight average molecular weight M_w was estimated by means of the equation (Ref. 2)

$$[\eta] = 4.13 \times 10^{-4} M_w^{0.64}$$

It has been shown (*SPS 37-16*, Vol. IV) that the ratio of the weight average molecular weight M_w, to number

average molecular weight M_n for most probable distributions is given by

$$M_w/M_n = 2/(1 + M_u/M_w)$$

or

$$M_n = (M_w + M_u)/2$$

Therefore, M_n was calculated from M_w and an assumed value of the unit molecular weight $M_u = 1100$, the average spacing of urethane links. The value of M_u was also used to calculate the number degree of polymerization X_n. In addition, the average number of cuts per molecule S, and the fraction of urethane links broken F, were calculated from

$$S = (X_{n(0)}/X_{n(t)}) - 1$$

and

$$F = S/(X_{n(0)} - 1)$$

in which $X_{n(0)}$ and $X_{n(t)}$ are the number average degrees of polymerization at time zero and time t, respectively. For a system undergoing strictly random degradation, the integrated rate equation is

$$-\log\left(\frac{X_{n(t)} - 1}{X_{n(t)}}\right) = -\log\left(\frac{X_{n(0)} - 1}{X_{n(0)}}\right) + kt$$

For such a process a plot of $-\log [(X_{n(t)}-1)/X_{n(t)}]$ versus time t, should give a straight line with a slope k and an intercept of $-\log [(X_{n(0)}-1)/X_{n(0)}]$ (Ref. 3).

The results for POPG–TDI and the POEG–POP–TDI polymers are given in Table 1 and Fig. 1, and the

$$-\log [(X_{n(t)}-1)/X_{n(t)}]$$

versus t plot in Fig. 2. It is apparent from the decrease in $[\eta]$ and the values of S and F that the initial rate of degradation is much less for the block polymer. Fig. 2

Table 1. Thermal degradation of POPG–TDI and a block (POEG–POP)–TDI polymer at 200°C under helium

Polymer	Time, min	Intrinsic viscosity,[a] $[\eta]$, dl/g	Weight average molecular wt,[b] $M_w \times 10^{-3}$	Number average molecular wt,[c] $M_n \times 10^{-3}$	Number average chain length,[d] X_n	$-\log \frac{X_n - 1}{X_n}$	Number of cuts,[e] S	Extent of degradation,[f] F
POPG–TDI	0	0.336	35.5	18.29	16.63	0.02664	0.0	0.0
	15	0.243	21.4	11.24	10.22	0.04455	0.6275	0.04015
	75	0.202	16.0	8.55	7.775	0.05973	1.140	0.07295
	135	0.195	15.0	8.055	7.322	0.06374	1.270	0.08125
	195	0.176	12.9	7.000	6.364	0.07417	1.613	0.1032
	255	0.166	11.7	6.400	5.816	0.08176	1.860	0.1190
	315	0.160	11.0	6.050	5.500	0.08725	2.025	0.1296
	375	0.153	10.4	5.750	5.227	0.09232	2.181	0.1395
	460	0.150	10.0	5.550	5.044	0.09583	2.297	0.1469
	1635	0.118	6.95	4.023	3.657	0.13847	3.548	0.2271
	3165	0.102	5.45	3.274	2.977	0.17751	4.585	0.2933
(POEG–POP)–TDI	0	0.478	62.0	31.55	28.69	0.01525	0.0	0.0
	15	0.450	56.0	28.53	25.95	0.01705	0.1060	0.03829
	75	0.409	49.0	25.04	22.77	0.01932	0.2590	0.009360
	135	0.371	41.8	21.45	19.50	0.02273	0.4710	0.01701
	255	0.229	19.5	10.30	9.370	0.04905	2.062	0.07450
	315	0.206	16.8	8.96	8.145	0.05690	2.522	0.09110
	375	0.190	14.6	7.850	7.138	0.06550	3.020	0.1091
	460	0.180	13.3	7.200	6.545	0.07186	3.383	0.1222
	1635	0.138	8.8	4.950	4.500	0.10902	5.378	0.1943
	3195	0.121	7.2	4.147	3.770	0.13401	6.610	0.2388

[a] Determined in benzene solutions at 25°C and calculated from $\eta_{sp}/c = [\eta] + k'[\eta]^2 c$, using $k' = 0.39$ (Ref. 1).
[b] From $[\eta] = 0.413 \times 10^{-4} M_w^{0.64}$.
[c] From $M_n = (M_w + M_u)/2$, assuming $M_u = 1100$.
[d] From $X_n = M_n/M_u$, assuming $M_u = 1100$.
[e] From $S = X_{n(0)}/X_{n(t)} - 1$.
[f] From $F = S/(X_{n(0)} - 1)$; F is the fraction of urethane bonds broken.

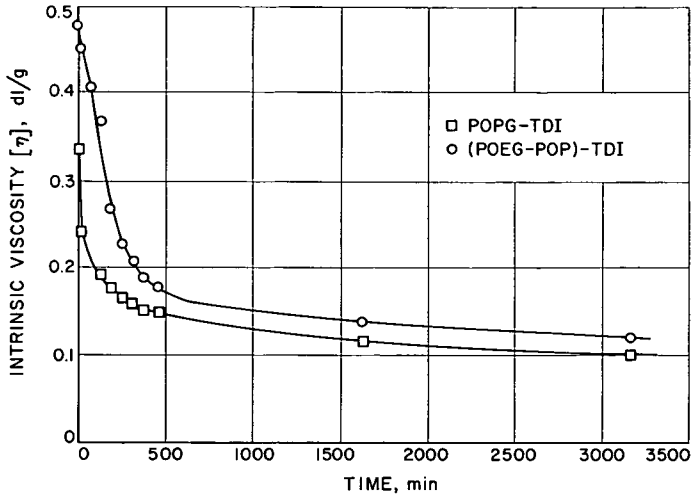

Fig. 1. Decrease of intrinsic viscosity on thermal degradation of POPG–TDI and block (POEG–POP)–TDI polymers at 200°C under helium

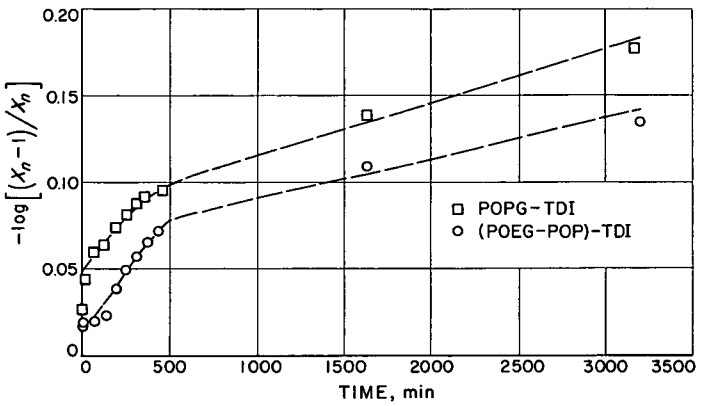

Fig. 2. Kinetic plot of thermal degradation of POPG–TDI and block (POEG–POP)–TDI polymers at 200°C under helium

shows that neither polymer exhibits strictly random degradation since the available cleavable bonds undergo scission at different decreasing rates as degradation proceeds. Extrapolation of the first straight line portion of the curve for POPG–TDI to zero time gives a molecular weight of 10,000, which represents the spacing of the very weak links. Since a similar extrapolation for (POEG–POP)–TDI gives the initial molecular weight, such weak links do not appear to be present in this polymer. The results indicate that the weak links involve terminal secondary hydroxyls on the POPG, presumably reacted with *ortho*-isocyanate groups. However, this must be regarded as a tentative conclusion based on a single experiment. One obvious objection that arises is that the weak bond spacing is too large if all the urethane bonds formed from secondary hydroxyl and *ortho*-isocyanate groups are involved, since such bonds are present in higher concentration than one per 5 POPG units. Since it is possible that a small contaminating precursor for weak link formation may have been removed from the POEG–PPG during block polymer preparation that was still present in the POPG control sample, further experiments will include parallel treatment of the POPG reacted with ethylene oxide and a control preparation omitting only the ethylene oxide addition. In addition, the degradation studies will be extended to lower temperatures in an attempt to determine the energy of activation for weak link scission in POPG–TDI polymer.

2. *The Huggins Constant k′ for POPG and Degraded POPG-TDI Polymers*

For benzene solutions of POPG–TDI at 25°C the Huggins Constant k' has been found to be ~0.39 for

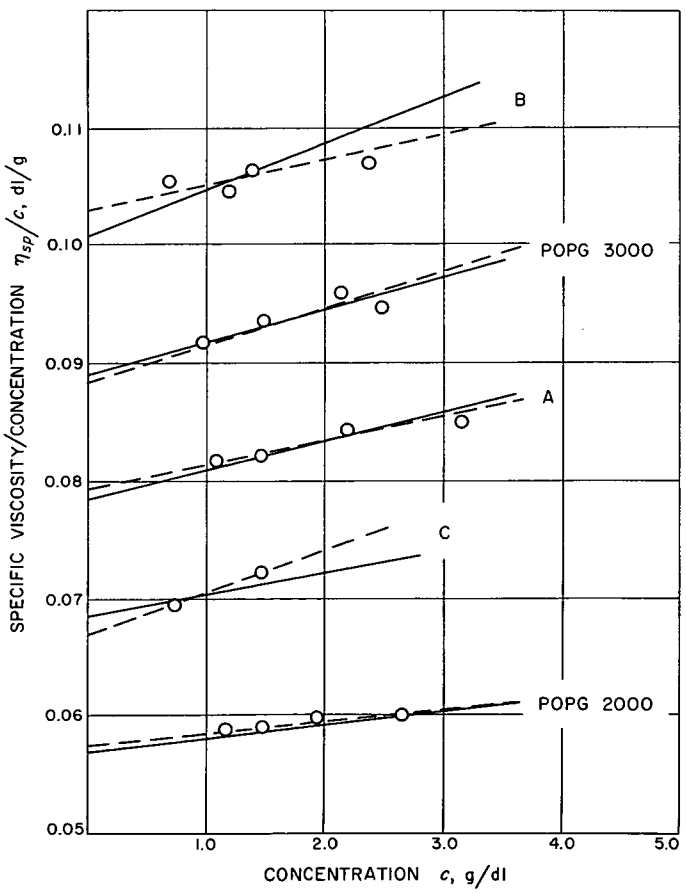

Fig. 3. Plots of η_{sp}/c versus c for POPG-2000, POPG-3000 and degraded POPG-TDI polymers A, B, and C

Table 2. Intrinsic viscosity measurements on POPG and degraded POPG-TDI polymers

Sample	Concentration c, g/dl	Specific viscosity η_{sp}	η_{sp}/c	Intrinsic viscosity[a] $[\eta]$, dl/g	Average intrinsic viscosity[a] $[\eta]$, dl/g	Intrinsic viscosity[b] $[\eta]$, dl/g	Constant[c] k' calculated
POPG-2000	2.65	0.158	0.0597	0.056	0.0570	0.0576	0.38
	1.93	0.115	0.0597	0.057			
	1.44	0.0852	0.0590	0.057			
	1.16	0.0682	0.0590	0.058			
POPG-3000	2.49	0.235	0.0946	0.087	0.0885	0.0883	0.43
	2.13	0.205	0.0959	0.089			
	1.49	0.140	0.0936	0.089			
	0.996	0.0914	0.0917	0.089			
A	3.14	0.266	0.0850	0.078	0.0785	0.0793	0.31
	2.20	0.185	0.0843	0.079			
	1.46	0.120	0.0821	0.078			
	1.098	0.0897	0.0817	0.079			
B	2.39	0.257	0.1072	0.098	0.1007	0.1027	0.21
	1.40	0.149	0.1064	0.101			
	1.20	0.126	0.1045	0.101			
	0.699	0.0738	0.1056	0.103			
C	1.46	0.105	0.0722	0.069	0.0685	0.0670	0.79
	0.728	0.0506	0.0695	0.068			

[a] These intrinsic viscosities were obtained by calculation assuming $k' = 0.39$ for each concentration.

[b] These intrinsic viscosities were obtained by extrapolation to infinite dilution from the plot of η_{sp}/c versus c.

[c] These values of k' were calculated from the equation $\eta_{sp}/c = [\eta] + k'[\eta]^2 c$ from the plot of η_{sp}/c versus c.

intrinsic viscosities from 0.1 to 0.6 (Ref. 1). In the present work this value has been assumed to be valid for POPG and highly degraded POPG–TDI polymers. Ordinarily η_{sp} is determined for two concentrations and $[\eta]$ calculated from $\eta_{sp}/c = [\eta] + 0.39[\eta]^2 c$. Since the two values of $[\eta]$ generally agree within 0.002 dl/g, use of $k' = 0.39$ is apparently justified. In an effort to determine an experimental value for k' and more adequately assess the possible errors resulting from the assumption that $k' = 0.39$ for POPG and degraded POPG–TDI polymers, some viscosity data at different concentrations have been obtained and are shown in Table 2 and Fig. 3. The solid lines in Fig. 3 have slopes such that $k' = 0.39$; the dashed lines were previously established from the experimental points. Although values of k' from the latter deviate widely from 0.39, the solid lines fit the data within the limits of error and the intrinsic viscosities obtained from either line agree within 0.002 dl/g. Therefore, use of $k' = 0.39$ for polymers of this type should not result in large errors in $[\eta]$. For a unique determination of the true values of k', more accurate data are required. Greater precision could be obtained by increasing the concentration to give higher relative viscosities; however, the results of Fig. 3 indicate that the η_{sp}/c versus c plots may not be linear at concentrations much greater ~2 g/dl.

B. A Study of the Ultimate Properties of Amorphous Gum Vulcanizates

R. F. Fedors and R. F. Landel

1. Introduction

An understanding of the molecular mechanisms which control the ultimate properties of elastomeric materials would be of considerable utility from the standpoint of both theoretical and practical applications. A working theory of the ultimate property behavior of vulcanizates would constitute a long step in contributing a basis for the design of polymeric materials to desired specifications; in addition, once the molecular basis for ultimate property behavior in amorphous gum vulcanizates is understood, then there will be sound basis for understanding the like behavior of filled systems. One pre-

requisite to the formulation or test of any theory is the collection of basic data on the behavior of well characterized vulcanizate systems.

The materials chosen for study are peroxide-cured rubber vulcanizates based on a low temperature styrene–butadiene copolymer generally designated as SBR-1500. The following recipe has been adopted for this study: 1 part Di-Cup R (Dicumyl peroxide) to 100 parts SBR-1500.

This report is concerned primarily with the evaluation and characterization of these specimens by means of "equilibrium" stress–strain, equilibrium swelling behavior, measurement of the sol fraction and measurement of the volume changes on extension.

2. Characterization of Cure

a. Equilibrium stress-strain. From the equation of state for rubber elasticity derived for an ideal rubber, the equilibrium relationship between stress σ_0, concentration of effective network chains per cc of rubber ν_e, and the extension ratio α, is given by (Ref. 3):

$$\sigma_0 = \nu_e RT\left(\alpha - \frac{1}{\alpha^2}\right), \qquad (1)$$

where R is the gas constant in the appropriate units and T is the absolute temperature. Equation (1) is generally found to describe experimental quasi-equilibrium data obtained with real rubbers to a good approximation where $\alpha < 2$. Hence, a plot of σ_0 against the quantity $[\alpha - (1/\alpha^2)]$ should be linear with slope directly proportional to ν_e. The data obtained for the various cures are shown in Fig. 4. The 45-min cure was run in duplicate and the agreement is satisfactory. From the slopes of the curves, the values of ν_e were calculated as a function of cure time and are shown in Fig. 5.

b. Equilibrium swelling. An alternative method of obtaining the concentration of effective network chains per unit volume of rubber is by equilibrium swelling measurements. It has been shown that the relationship between volume fraction of gel in the swollen vulcanizate, v_2 and ν_e for an ideal rubber is given by (Ref. 4, 5, 6):

$$\nu_e = -\frac{(1-s)}{V_0\left[v_2^{1/3}(1-s)^{2/3} - \frac{v_2}{2}\right]} \times \left\{\ln(1-v_2) + v_2 + \sum_{i=1} \chi_i v_2^{i+1}\right\} \qquad (2)$$

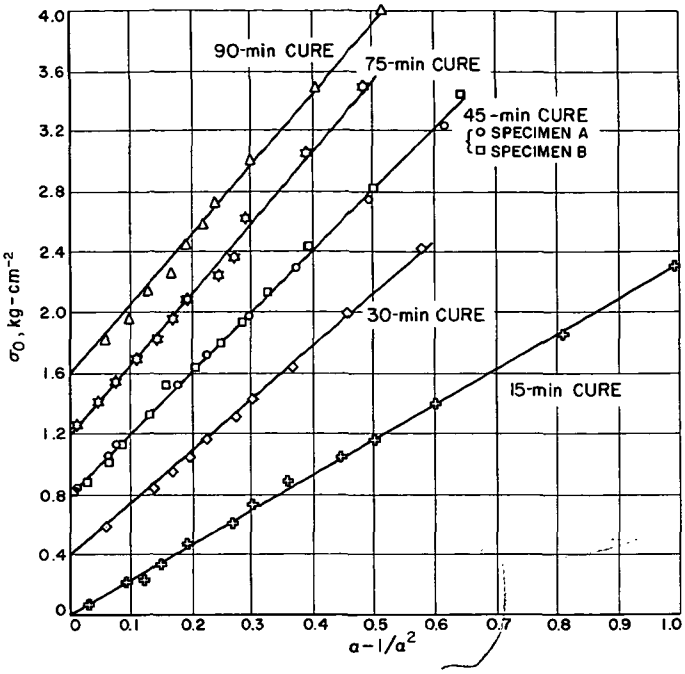

Fig. 4. Stress σ_0, as a function of the form factor $[\alpha - (1/\alpha^2)]$, for different cure times of an SBR-peroxide vulcanizate cured at 150°C

where $\chi_1, \chi_2, \chi_3, \cdots$, essentially represent polymer–solvent interaction coefficients, V_0 is the molal volume of

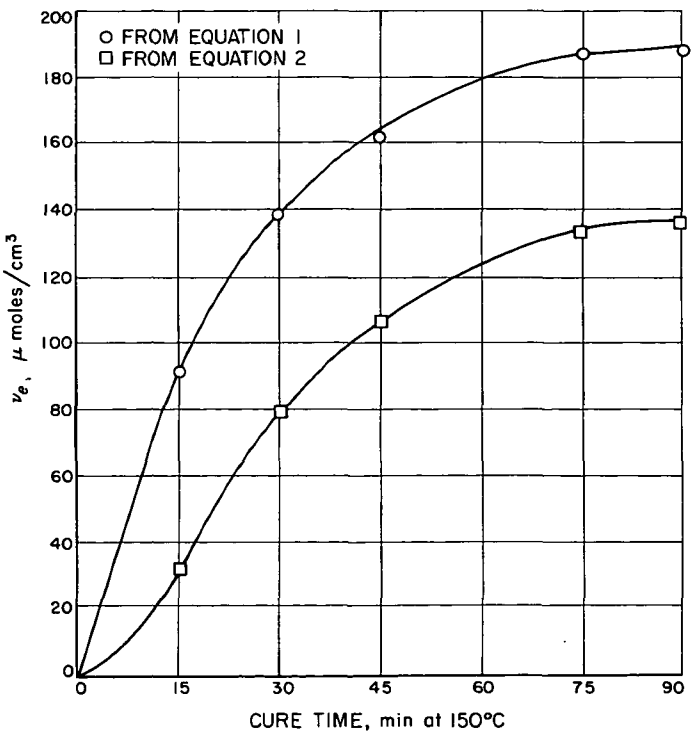

Fig. 5. Dependence of concentration of effective network chains ν_e, on cure time

solvent which for benzene at 23°C is 89.4 $cm^3\ mole^{-1}$, s is the sol fraction and v_2 is the volume fraction of gel rubber in the swollen vulcanizate. The calculated values of ν_e using $\chi_1 = 0.34$ as reported by Smith (Ref. 7) and taking $\chi_2, \chi_3, \cdots = 0$ are shown in Fig. 5.

The divergence between ν_e calculated from the kinetic theory expression, Eq. (1) and ν_e calculated from equilibrium swelling, Eq. (2) is presumably due to two major factors: (1) degradation of the swollen vulcanizates, and (2) the effect on swelling of the nature of the solvent used (Ref. 9). Both sets of data, however, allow an unambiguous selection of the "optimum cure" which for this system turns out to be 75 min. At the optimum cure, changes in the physical properties due to small variations in cure time are at a minimum.

c. Sol-gel ratio. The measured sol fraction as a function of cure time is shown in Fig. 6. In both theory and practice, the partition of polymer molecules between the sol and gel fractions is an important measure of network properties. The sol-gel relationships are particularly simple for the case of the cross-linking of linear primary molecules having a most probable distribution of molecular weights. For this information to be of value, the sol must be a true measure of soluble polymer. It can be shown that the experimental values of s are too large by a factor of about 5. This discrepancy is directly attributable to the extraneous materials such as fatty acids, antioxidants, etc., which are present in the raw polymer before vulcanization.

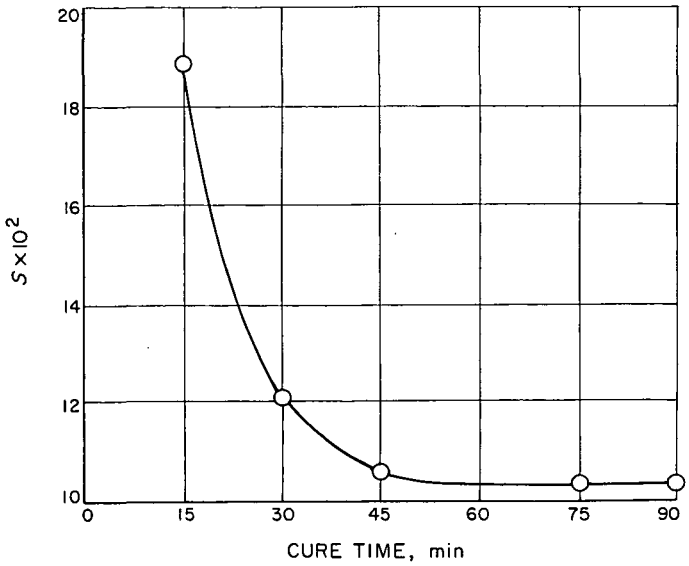

Fig. 6. Fraction of soluble material as a function of cure time

3. Physical Properties

a. Volume changes on extension. For the intended study of ultimate property behavior it is important to have knowledge of the change in volume on extension, especially for extensions approaching the ultimate. The method of hydrostatic weighing was used as a measure of volume changes. A rig was made up whereby four tensile ring specimens could be stretched under water in 0.5-in. increments. The totally immersed rig and either relaxed or extended specimens were suspended by a 10-mil platinum wire from a Mettler balance which was mounted on an essentially vibration-proof table. The results are shown in Fig. 7, where the weight of the immersed rig and specimens is shown as a function of time of immersion and extension ratio of the specimens. The filled circles represent the weight of relaxed specimens; the other symbols denote the weight at the various extension ratios. The change in weight on extension was taken as the difference in weight of the extended specimens and the weight of the relaxed specimens as interpolated from the linear portion of the curve.

Relative volume changes with extension are shown in Fig. 8. Data are also shown for SBR-peroxide vulcanizates (Ref. 11) and for natural rubber peroxide vulcanizate (Ref. 10) taken from the literature. Few data are available for comparison at large extension ratios, but Kusov et al. (Ref. 12) have also reported that the relationship between relative volume and strain yields an S-shaped curve.

The specimens ruptured at $\varepsilon = 3.1$, and even at break, the change in volume is only of the order of 0.06%. From the data of Fig. 8, values of the logarithmic Poisson ratio at various strains were calculated from (Ref. 8):

$$\frac{d(\ln V/V_0)}{d(\ln\lambda_1)} = 1 - 2\nu \qquad (3)$$

where V is the volume at any extension ratio λ_1, V_0 is the volume of the unstrained material and ν is Poisson's ratio. The results are shown in Fig. 9. It is to be expected that volume changes on extension will become more and more significant as the temperature decreases, i.e., as T_g is approached. Poisson's ratio should decrease from 0.5 to about 0.3 (Ref. 13). Therefore, volume changes on extension will be measured at selected low temperatures.

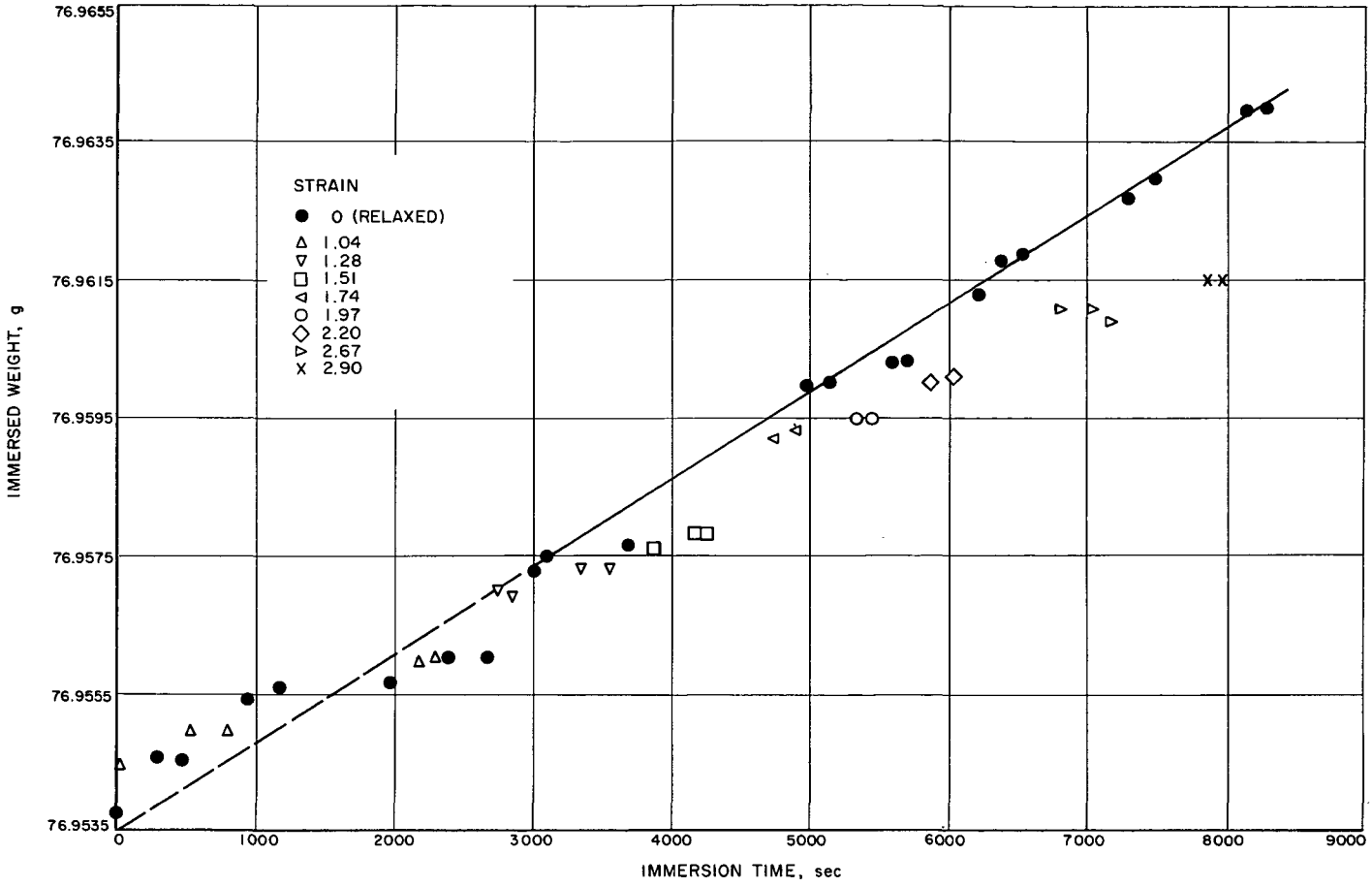

Fig. 7. Dependence of immersed weight on immersion time and strain

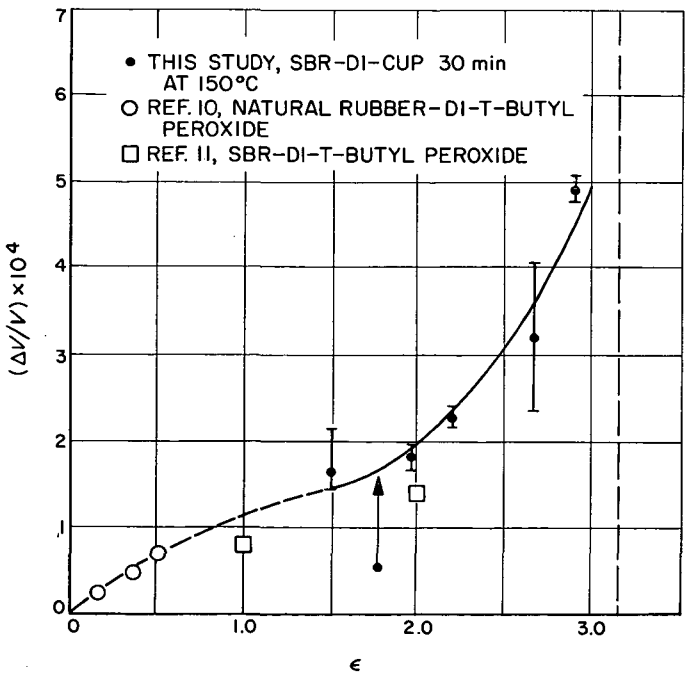

Fig. 8. Change in relative volume as a function of strain

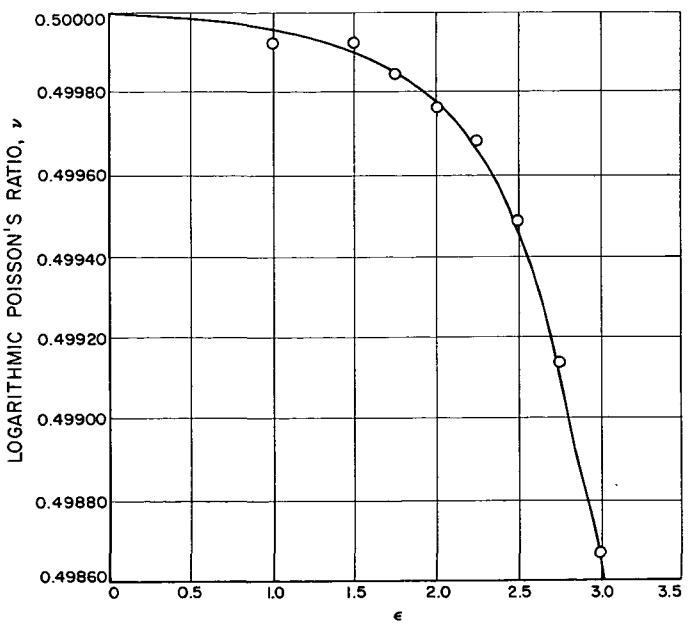

Fig. 9. Logarithmic Poisson's ratio ν, as a function of the strain ε

C. Continuous Medium Theory Applied to Viscoelastic Strain Analysis, II

A. San Miguel

A study program of solid propellant viscoelastic physical properties is being formulated from a different point of view. The apparently divergent previous studies (*QSR 38-3* through *QSR 38-9*) shall now begin to converge with this report. Since our approach to the problem of viscoelasticity is somewhat different from the approach used by the majority of investigators, seemingly unrelated parallel studies will be conducted in the future to either confirm or deny the hypotheses used in this study. The study reviewed in this report was presented last October at the 33rd annual meeting of the Society of Rheology (Ref. 14). Since the basic ideas incorporate a relatively unfamiliar complement of higher mathematics and experimentation, other investigators should not extrapolate conclusions until any discrepancies that may arise in the immediate future are resolved.

A preliminary introduction to Continuous Medium Theory was presented in *QSR 38-7*. Studies were initiated to determine the applicability of Continuous Medium Theory to propellant viscoelastic strain analysis. Topics discussed introduced concepts pertaining to: the physical significance of a strain energy function W with respect to propellant, a hypothesis specifying $\varepsilon_{33} = 0$ on the boundary at the free end surface of a biaxially pressurized propellant grain specimen, a comparison of this hypothesis with the generally accepted assumption that ε_{33} is equal to an average structural strain, the relationships between the various cartesian strain invariants, I_1, I_2, I_3, and, finally, the introduction of time dependency into the strain energy function.

This report will review the mathematics involved and the experimental data that are necessary to evaluate the strain energy function W. The amenability of the photoelastic coating technique (*QSR 38-3* through *38-9*) to Continuous Medium Theory is apparent since the underlying mathematical assumptions regarding "point" strains in the theory are satisfied by the technique. Experimental correlations between triaxial point strains and the strain energy function as a function of time will be reported at a later date.

1. Further Observations

The strain energy function will continue to be expressed in terms of two longitudinal surface strain hypotheses ($\varepsilon_{33} = 0$; ε_{33} = average structural strain) for the measured longitudinal principal strain (ε_{33}) for the time being (*QSR 38-7*). Comparisons with derived strain energy functions studied at this Laboratory using these assumptions will eventually be compared to analogous strain energy functions obtained under different assumptions, e.g., Refs. 15, 16, 17.

The importance of an explicit experimental strain hypothesis is evident if the generally accepted mathematical interpretation of physical properties based on a point strain concept is to be utilized. The experimental difficulty of measuring the three principal strains at a point region in a solid propellant has not as yet been completely overcome. It is common practice for investigators to choose specific structures, e.g., JANAF tensile bars, and assume strain relationships based on homogeneity, isotropy, etc. Usually an experimentalist assumes some form of a stress-strain law to be valid. This law may be represented by a set of constitutive equations. The law will inherently define certain relationships to exist between the various principal strains. Apart from the fact that the law may also contain some inherent assumptions as well, e.g., homogeneity, isotropy, or linearity, which are violated by the real material, it is also possible that the experimental stress-strain relations cannot be fulfilled except by allowing one or more of the constants of the assumed stress-strain law to become a variable, e.g., a variable Poisson's ratio. Under these circumstances it would appear that the initial assumption of the law is not correct, and thus use of the initial equations is not entirely justified except as an *ad hoc* relationship with no explicit theoretical basis.

Another difficulty is that boundary effects always exist, and while there may be ways of avoiding them, it seems unwise or unwary to attempt to describe physical behavior without first insuring that these extraneous effects are either truly negligible or are properly accounted for in the theoretical description or analysis of the experiment.

It has been observed that boundary effects are commonly neglected in the propellant literature. All experimental data (deformations of structure) inadvertently contain these effects to some degree. One alternative commonly employed is to make certain strain measurements, average them, and apply them to a defined area or volume. The JANAF tensile bar experiment is an example.

A difficulty is sometimes encountered in the use of average or structural strains in lieu of point strains. While it is true that the over-all deformation is merely the

integrated result of all strains, it is not precise to take the average deformation as equal to the point strains. In the literature, such boundary effects are ignored regardless of the problem under investigation.

It has been observed at this Laboratory and elsewhere that, for even a tensile bar, the two principal strains vary somewhat both in direction and magnitude at various points on the propellant surface within the nominal gage length. The primary cause of this observation is probably due in part to sample preparation (machining, Ref. 18) or inadequate instrumentation. Observations of physical failure surfaces, such as the fractured jagged surface of a tensile bar, indicate that the principal strain fields possibly rotate, or that the individual principal point strains constantly change in magnitude, or both. It is noted that the mechanics of fracture is generally indeterminate. In summary, even with this relatively simple experiment, a variably stressed structure was employed in conjunction with a theory derived for point analysis.

To avoid some of the above difficulties, the experimentalist should: (1) use a relationship between stress and deformation which is as unrestrictive as possible (the strain energy function W, discussed below, will be used), (2) examine test specimens carefully for boundary effects and try to either eliminate them or learn how to live with them by reducing their effect on measurements or by accounting for them in the stress-strain relationship, and (3) use a point strain and stress measuring technique.

An experimental requirement which satisfies the assumptions underlying the mathematics of a strain concept is that each of the three principal strains be measured in a point region of the material. Approximations to this

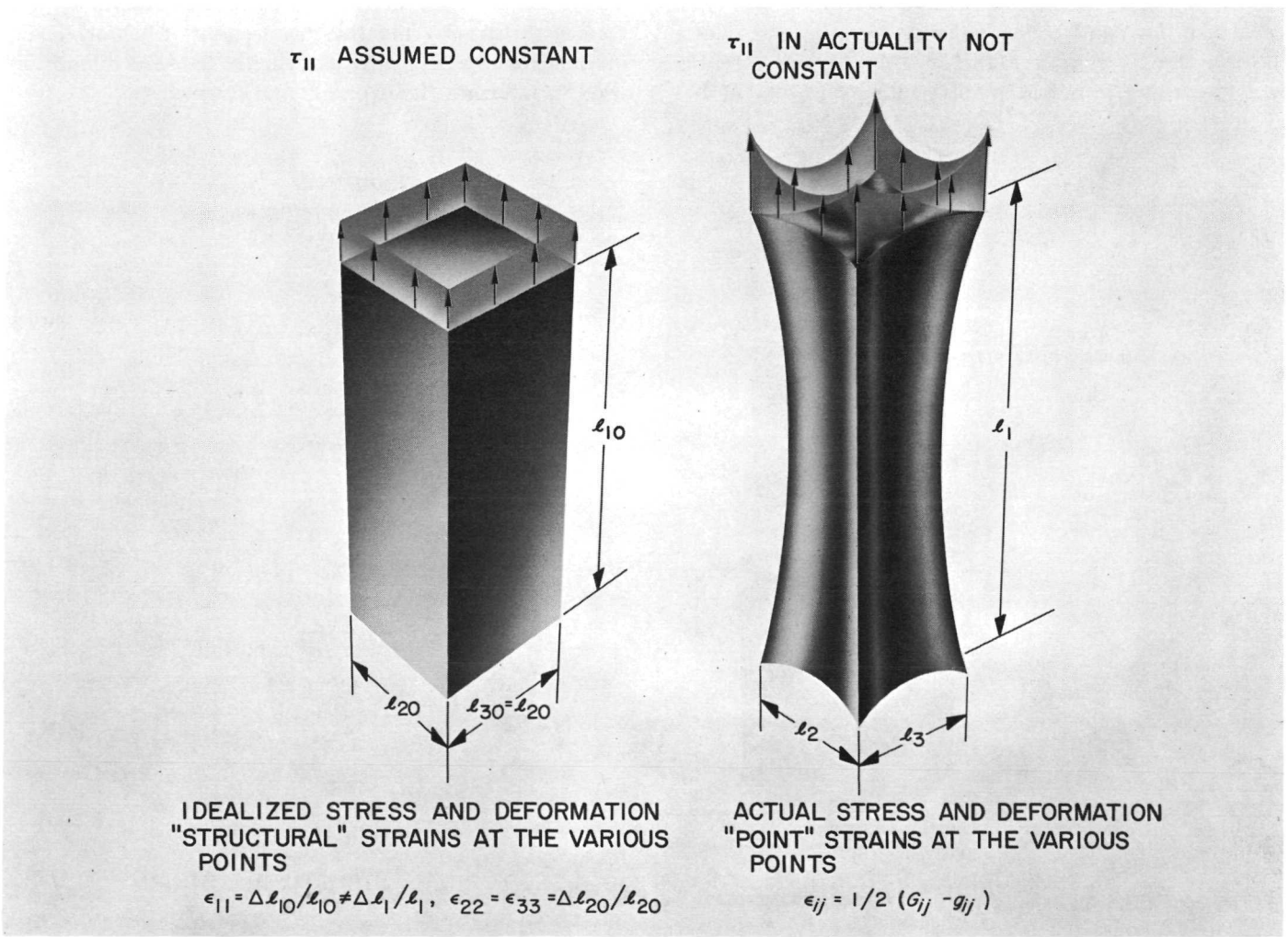

Fig. 10. Exaggerated deformation comparisons of tensile bars at large strain levels

requirement are found in contemporary bi- and tri- axial experiments (Ref. 19). Usually in these experiments two structural deformation measurements are made, and the three principal point strains are deduced by assumptions. In some,propellant physical property experiments, most, if not all measured principal strains are in actuality average structural strains, i.e., boundary deformations are measured. Fig. 10 illustrates an exaggeration of this statement for a tensile experiment. Needless to say, for such an experiment the concise geometric expression for volume is indeed quite difficult to express mathematically in terms of principal point strains. These actual strains are usually erroneously presumed constant in direction and magnitude at any point throughout the structure, although, in the aggregate, this discrepancy may be trivial for macroscopic analysis.

Problems relating experimental strain to mathematical strain are being reviewed at this Laboratory. Currently it is found that measurement of biaxial point principal surface strains can be accomplished by using the photoelastic coating technique (*QSR 38-3* through *38-9*). However, the third principal point strain measurement has not as yet been resolved and is a problem under current investigation. For expediency, until the aforementioned problem is solved, the third principal strain shall be taken as equal to the average structural longitudinal strain $\varepsilon'_{33} = \Delta l'_{33}/l'_{33}$, Hypothesis I (Fig. 11); and as being equal to zero at the free end surface of the biaxially pressurized grain $\varepsilon_{33} = 0$, Hypothesis II. These two hypotheses define the extreme values that the longitudinal strain can assume. It is noted that experimental circumstantial evidence exists that favors Hypothesis II. However, for the present time both hypotheses will be used with impartiality. The current extensometer used to measure this longitudinal structural strain is shown in Fig. 12. One should be aware of the experimental observation that an unrestricted biaxially pressurized cylinder bows in the center (Fig. 11). This effect is quite apparent for an unrestricted 5-in. D and 5-in. long propellant grain. If a small specimen is used in an experiment, naturally these extraneous effects are not obvious. However, they still exist and must be accounted for in the mathematical concept of strain. Thus the strain energy function development reported below will explicitly state the hypothesis used to interpret the experimental strain data.

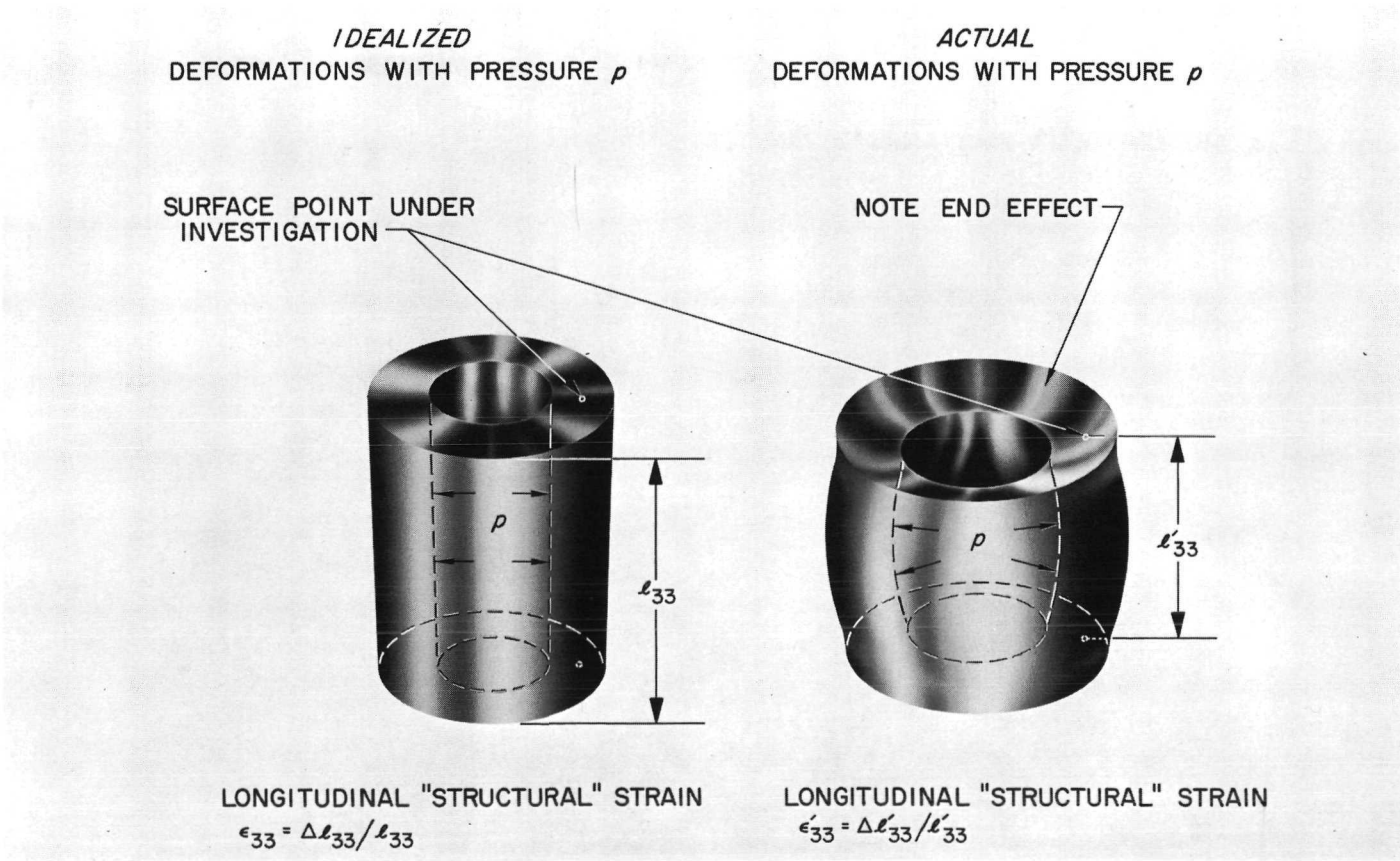

Fig. 11. Exaggerated deformation comparisons of an unrestricted thick wall cylinder at large strain levels

CONFIDENTIAL

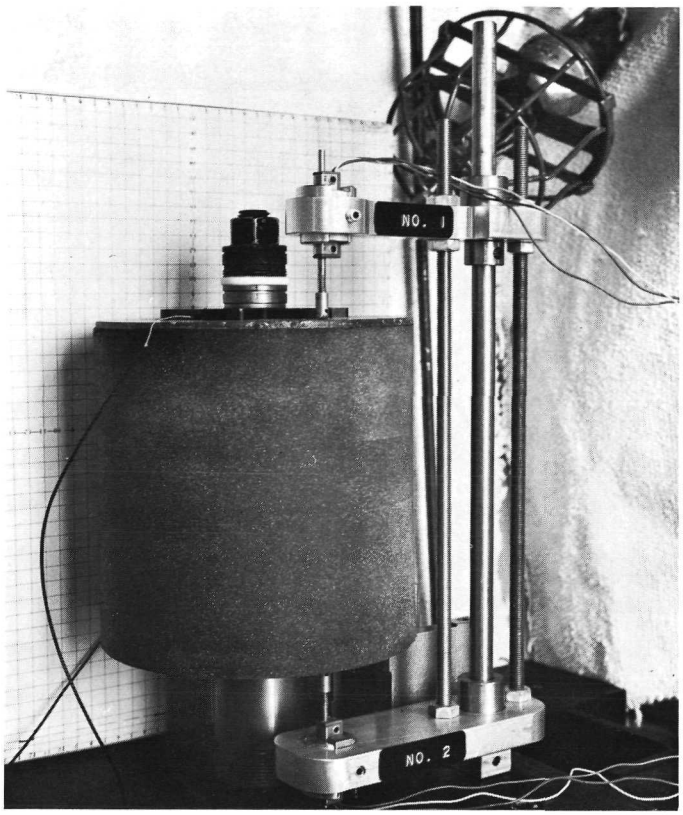

Fig. 12. Longitudinal extensometer to measure cylinder contraction and end deformations

2. The Derivation of the Strain Energy Function W

Experimental evidence is found in Ref. 20 for PBAA propellant that is in agreement with observations for polyurethane propellant; namely, that solid propellant exhibits a complete time-dependent elastic recovery when unloaded. Agreement is also found in Ref. 21 with observations for polyurethane propellant: this propellant will phenomenologically reheal itself. Creep data obtained at this Laboratory substantiate these preceding remarks. These two observations tend to encourage the concept that a time-dependent strain energy function may describe the viscoelastic[1] physical properties of solid propellant. There is good reason to believe that solid propellant inherently exhibits a recoverable memory which is analogous to a time-dependent strain energy function. The mathematical derivation of such a strain energy function is presented below for any given instant in time. At a later date, these equations will explicitly include a time function. Experimental data is currently being accumulated for this purpose.

In *QSR 38-7* it was proposed that the constitutive equation for a continuous medium of solid propellant (in the macroscopic sense) be

$$\tau^{ij} = \frac{1}{2}\left(\frac{g}{G}\right)^{1/2}\left\{\frac{\partial W}{\partial I_1}\left(\frac{\partial I_1}{\partial \varepsilon_{ij}} + \frac{\partial I_1}{\partial \varepsilon_{ji}}\right) + \frac{\partial W}{\partial I_2}\left(\frac{\partial I_2}{\partial \varepsilon_{ij}} + \frac{\partial I_2}{\partial \varepsilon_{ji}}\right) + \frac{\partial W}{\partial I_3}\left(\frac{\partial I_3}{\partial \varepsilon_{ij}} + \frac{\partial I_3}{\partial \varepsilon_{ji}}\right)\right\} \quad (1)$$

where

τ^{ij} = contravariant stress tensor

$g = |g_{mn}|$ = covariant metric tensor (unstrained state; g is the determinant of the array g_{mn}

$G = |G_{mn}|$ = covariant metric tensor (strained state; G is the determinant of the array G_{mn})

$W(I_1, I_2, I_3, x) = \rho U(I_1, I_2, I_3, x)$ = elastic potential per unit volume of the unstrained body

ρ = density of the propellant

$U(I_1, I_2, I_3, x)$ = internal energy in the classical thermodynamic (thermostatic) sense

x = independent variable such as entropy or time

I_1, I_2, I_3 = strain invariants. For the deformation where a cube deforms into a cuboid and the material and space coordinates are cartesian

$I_1 = \lambda_1^2 + \lambda_2^2 + \lambda_3^2$

$I_2 = \lambda_1^2\lambda_2^2 + \lambda_1^2\lambda_3^2 + \lambda_2^2\lambda_3^2$

$I_3 = \lambda_1^2\lambda_2^2\lambda_3^2$

$\lambda_i = 1 + \varepsilon_{ii}$ = extension ratios

$\varepsilon_{ij} = \varepsilon_{ji}$ = finite strain tensor

This equation was derived by assuming that the constitutive equation for solid propellant can be reasonably expressed in the form

$$\tau^{ij} = \rho \frac{\partial U}{\partial \varepsilon_{ij}} \quad (2)$$

It is noted that the time element can be arbitrarily introduced into Eq. (2) by simply suggesting that

[1]In the propellant field there is a tendency to describe time-dependent physical properties as being viscoelastic. It should be pointed out that in the field of rheology, time-dependent physical properties may be described as being anelastic, plastic-dynamic, etc. (Ref. 22).

CONFIDENTIAL

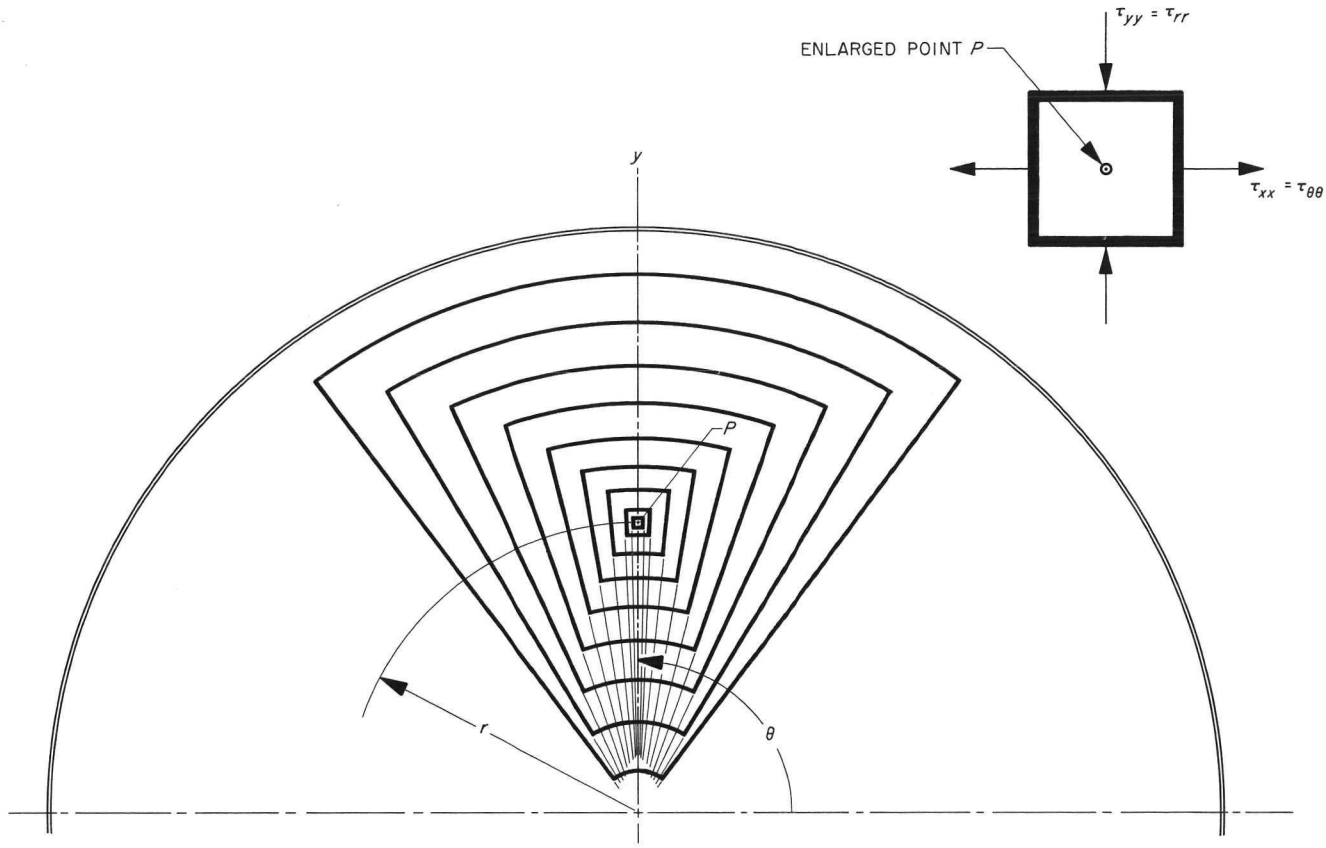

Fig. 13. An infinitesimal cube within a structure normally described by curvilinear coordinates

$U = U(t)$. All that was done here was to assume that the independent variable is time-dependent. This approach is sound, since any constitutive equation is of an intrinsic nature and can only make sense if the physical material under investigation happens, perchance, to satisfy the postulated relationships. A comprehensive treatise of this entire subject is found in Ref. 23.

Thus, if for the present, only the isochronal case is considered, and the stress-strain response of a cube into a cuboid is observed, then Eq. (1) reduces to

$$\tau_{ij} = \frac{1}{(I_3)^{1/2}}\left\{\frac{\partial W}{\partial I_1}\frac{\partial I_1}{\partial \varepsilon_{ij}} + \frac{\partial W}{\partial I_2}\frac{\partial I_2}{\partial \varepsilon_{ij}} + \frac{\partial W}{\partial I_3}\frac{\partial I_3}{\partial \varepsilon_{ij}}\right\} \quad (3)$$

The stress-strain response of various classes of continuum, such as rubbers, may be reasonably described by a constitutive equation of this form (Ref. 24, 25).

Ideally this constitutive equation is applicable to materials that exhibit perfect elasticity. Its superiority to classical elasticity is founded on its capability to incorporate both physical and geometric nonlinearity (Ref. 23). In addition, this constitutive form may also be empirically exploited for materials whose energy function is dissipated in some prescribed manner.

For an isotropic material subjected to a three-dimensional strain field Eq. (3) reduces to six equations containing 33 unknowns (6 stresses, 6 strains, 18 invariant gradients, and 3 potential gradients). The strain energy function W must experimentally satisfy all six of these equations. Thus, the experimental task was to obtain a sufficient number of values for the 30 physical parameters at various points on a medium in order to be able to solve for the three potential gradients

$$Ю = \frac{\partial W}{\partial I_1}, \quad И = \frac{\partial W}{\partial I_2}, \text{ and } \quad Я = \frac{\partial W}{\partial I_3}$$

Our approach will be to work directly from Eq. (1) using a relatively complex three-dimensional strain problem. The structure to be investigated is a radially pressurized, unrestricted thick-walled cylinder. This geometry was chosen because the principal stresses at a point may be reasonably approximated for finite strains (to 30%) independently of the medium's physical properties. The

CONFIDENTIAL

major change in approach from that of earlier work, is that two of the three principal strains are not computed from boundary motions (i.e., from structural deformations), which shall be called structural strains. Instead, biaxial principal strains are measured *at a point* on the cylinder end surface, using a birefringent, low-modulus coating. The third principal strain, always relatively small, was measured as a structural strain by following the axial motion of the cylinder with an extensometer. The entire data reduction process, tedious but not complex, was amenable to computer solution for obtaining the magnitudes of Ю, И, Я at various points on the cylinder. The strain energy function W was then calculated from these gradients for a polyurethane propellant.

3. Stresses

To be consistent with point analysis, it would be necessary to know the principal stresses at the same point that the strains are measured. Experimentally, only structural boundary stresses may be measured with any degree of accuracy. Although there are internal stress-measuring devices currently available (e.g., various semiconductors), most suffer from not being able to measure explicitly the true principal stresses and their directions. One fault of these gages is that they introduce unknown discontinuities (stress concentrations) in the medium under investigation. Therefore, it would be expedient to design an experiment where only the external structural boundary stresses (applied loadings) are measured and the internal point boundary stresses are calculated; with respect to an infinitesimal cuboid. This may be accomplished by taking advantage of the fact that in the limit, principal stresses at a point in curvilinear coordinates are identical to principal stresses in cartesian coordinates. It can be shown that such a multiaxial principal stress field at a point which describes the boundary stresses of an infinitesimal cuboid may be described for a structure whose geometry is normally characterized in terms of curvilinear coordinates.

The only reason to choose a curvilinear system for a symmetrical geometry is that it is simpler to express the boundary conditions of a vector field in natural coordinates. There is no reason to generalize our thinking to a curvilinear system for the geometry in question, a thick-walled cylinder.

Upon examination of Fig. 13, one notes that in the limit, the orthogonal net dr, $rd\theta$ approaches dx, dy. By definition, τ_{ii} is a tensor unique to the point under investigation. It is also recalled that the scalar value of a tensor is invariant with respect to the reference coordinate system. Thus, at a point

$$\tau_{xx} = \tau_{\theta\theta} \ , \ \tau_{yy} = \tau_{rr} \ , \ \tau_{zz} = \tau_{zz}$$

Consider the classical theoretical equations for an internally pressurized unrestricted thick wall tube subjected only to a biaxial radial pressure (Fig. 14). The equations that describe the stress state at various points *independent of the medium's physical properties are*

$$\overset{i}{\tau}_{11} = \frac{a^2 p}{b^2 - a^2}\left(1 + \frac{b^2}{y_i^2}\right)$$

$$\overset{i}{\tau}_{22} = \frac{a^2 p}{b^2 - a^2}\left(1 - \frac{b^2}{y_i^2}\right)$$

$$\overset{i}{\tau}_{33} = 0 \qquad (4)$$

where

$\overset{i}{\tau}_{11}, \overset{i}{\tau}_{22}, \overset{i}{\tau}_{33}$ = point principal stresses at i

a = inner radius of cylinder

b = outer radius of cylinder

p = radial internal pressure

y_i = radial length to point under investigation

Strictly speaking, these equations[2] may be exactly valid only for infinitesimal strains. It is noted that Eq. (4) was derived by selecting a stress potential that explicitly satisfied the equilibrium equations. The compatibility equations for infinitesimal strains were then used to select a specific potential. But the specific potential function selected does not necessarily satisfy the compatibility equations for finite strains. No attempt has been made in this report to verify this specific function because of the complexity of the finite compatibility equations.

[2]It has been argued that these equations hold only for a plane uniform deformation (plane strain) in the longitudinal direction. This is *not* true. In the plane stress derivation, the components u, v, w of the displacement vector are not in general independent of z. Thus the plane stress problem is not a truly two-dimensional problem. From the equilibrium equations (by Airy Stress function) one obtains stresses in terms of three constants and two boundary conditions. It is at this point that inspection of the plane strain restriction reveals that one of the constants must be zero in order to satisfy single valueness for the displacement. However, this latter restriction should have been obvious since a real material is being used that contains no significant discontinuities in the macroscopic sense.

CONFIDENTIAL

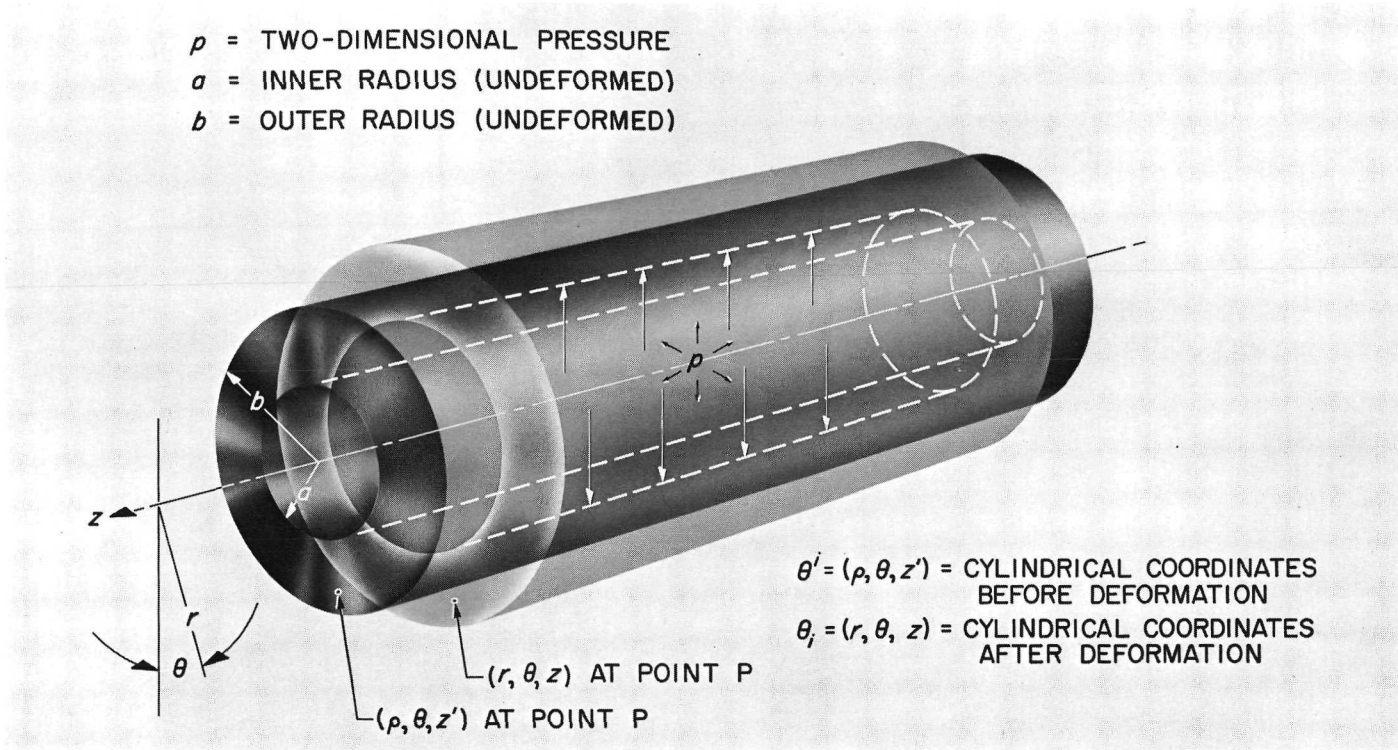
p = TWO-DIMENSIONAL PRESSURE
a = INNER RADIUS (UNDEFORMED)
b = OUTER RADIUS (UNDEFORMED)
θ' = (ρ, θ, z') = CYLINDRICAL COORDINATES BEFORE DEFORMATION
θ_i = (r, θ, z) = CYLINDRICAL COORDINATES AFTER DEFORMATION
(r, θ, z) AT POINT P
(ρ, θ, z') AT POINT P

Fig. 14. Idealized deformations of a biaxially pressurized unrestricted thick wall cylinder

On the other hand, the magnitude of internal stress errors that may be introduced because of finite strains (to 30%) should in all probability be negligible. This is because the equilibrium equations are satisfied at the boundaries regardless of the strain magnitude. Since the stresses are continuously increasing or decreasing, the mode between the boundaries would not be expected to deviate significantly. In any event, it is surmised that Eq. (4) would be applicable to finite strains if an iteration of the dimensions a and b is performed from strain level to strain level. Thus, point stresses can be obtained from the applied pressure, the cylinder dimensions, and the point coordinates.

Unpublished experimental studies of contained grains at this Laboratory have indicated that this potential function seems to satisfy the compatibility equations for strain magnitudes of at least 15%. The least qualifying argument in favor of the stress potential approach is that most of the popular analytical and experimental conclusions regarding structural analysis of rocket grains (static or viscoelastic) are based on such an approach. It is noted at this point that an infinitesimal stress-measuring device is under current study at this Laboratory to resolve this question.

4. The Concept of Strain (Ref. 23)

Care must be taken to not apply "strain" data indiscriminately to Eq. (3). Experimental strain data must conform to the metric tensor both before and during deformation. This required congruency arises from the mathematical definition of strain. This definition is not simply

$$\varepsilon_{mn} = \frac{\Delta l_{mn}}{l_{mn}} \tag{5}$$

but

$$\varepsilon_{mn} = \frac{1}{2}(G_{mn} - g_{mn}) \tag{6}$$

In continuum theory, the strains are defined as being one-half the difference of the corresponding components in the deformed G_{ij} and undeformed g_{ij} metric tensors (Ref. 24). The physical significance of such a definition is vague except for the strain representation of a cube

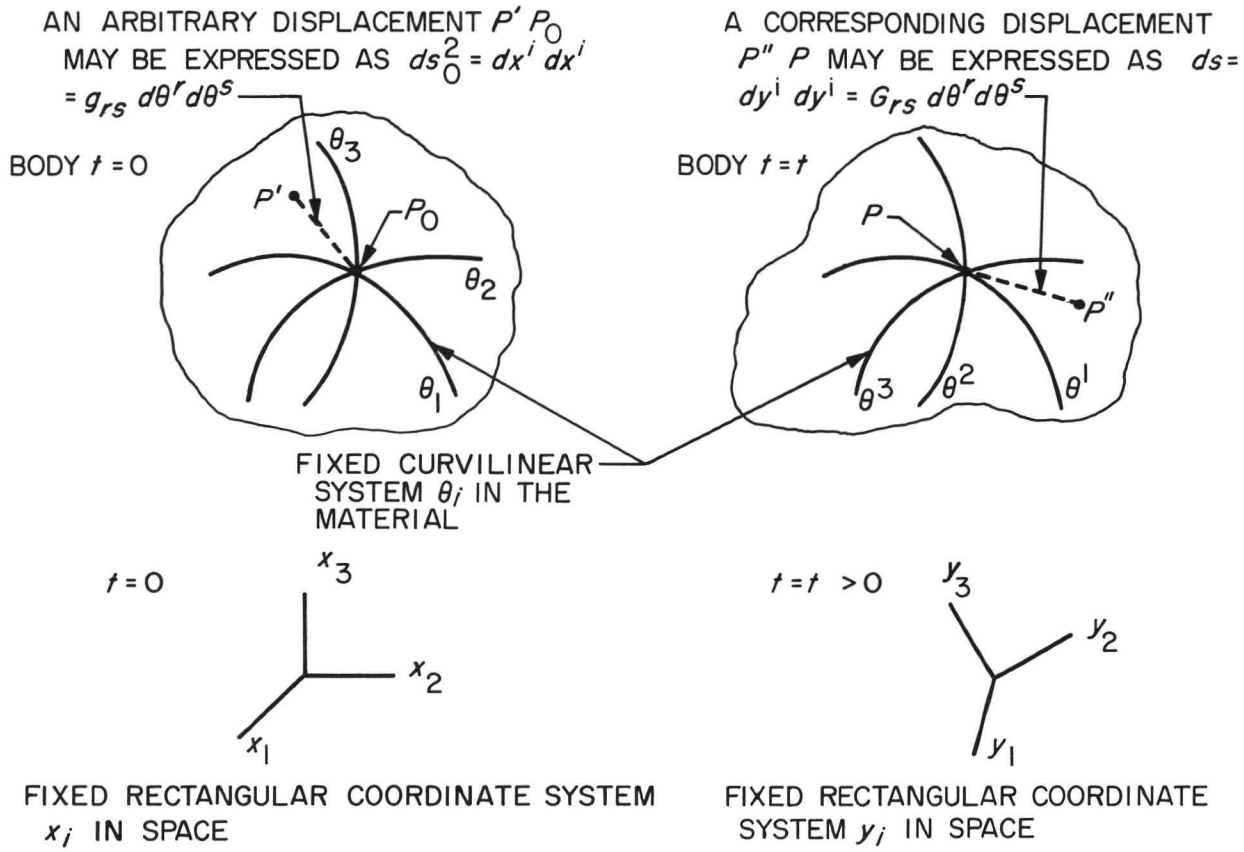

Fig. 15. The geometric concept of strains in a Euclidean space

which deforms into a cuboid in cartesian coordinates. Mathematically the strain is then defined for the irrotational condition as

$$\varepsilon_{11} = \frac{\partial u}{\partial x} + \frac{1}{2}\left(\frac{\partial u}{\partial x}\right)^2$$

$$\varepsilon_{22} = \frac{\partial v}{\partial y} + \frac{1}{2}\left(\frac{\partial v}{\partial y}\right)^2$$

$$\varepsilon_{33} = \frac{\partial w}{\partial z} + \frac{1}{2}\left(\frac{\partial w}{\partial z}\right)^2 \qquad (7)$$

where u, v, and w are the displacement components of the points on the body being deformed.

A distinction is here made between the point strain defined by Eq. (7) and the structural strain that is usually measured in the laboratory. As pointed out by Rivlin (Ref. 25), "One of the major difficulties is to perform an experiment of desired pure homogeneous deformations which is uncomplicated by end (boundary) effects." To circumvent the distinctions between point and structural strains requires that strain measurements be made at a point in or on the medium being examined. The magnitude of such a measured strain must equal ε_{ii} and satisfy the displacement gradients.

Following the same line of reasoning presented above for stresses, it is obvious that the point strains in a pressurized cylinder may be reasonably described in terms of an infinitesimal unit cube structure that deforms into a cuboid of extensions λ_1, λ_2, λ_3.

At this point attention is brought to Ref. 26. An excellent introduction to tensor calculus and engineering solutions of such mathematics is found in this reference, which can facilitate the interpretation of the voluminous mathematical theory available in the literature and in Refs. 14–29.

The mathematical concept of strain is generally presented as follows: Figure 15 illustrates two points P_0

and P existing in a Euclidian space. It is assumed that P at time t is related to P_0 at time $t = 0$ by

$$y_i = y_i(x_1, x_2, x_3, t)$$

$$x_i = x_i(y_1, y_2, y_3, t) \tag{8}$$

Obvious assumptions regarding single-valueness and continuous differentiability are made. It is also assumed that differentials dy^i, evaluated at some time t, may be expressed in terms of differentials dx^j by

$$dy^i = \frac{\partial y^i}{\partial x^j} dx^j \quad , \qquad dx^i = \frac{\partial x^i}{\partial y^j} dy^j \tag{9}$$

In tensor calculus a distinction is made between subscripts and superscripts on differential variables. The former is associated with covariant differentiation and the latter with contravariant differentiation. In a rectangular coordinate frame, no distinction is made between covariant and contravariant tensors.

As the body is deformed, depending on its physical properties, arbitrary points P' about P_0 and P'' about P are relatively relocated in some manner in the displacement process giving rise to $ds \neq ds_0$. The propellant is said to be strained in the ds position.

In mathematical terms the dot product of the base vectors to an orthogonal net (frame or system) is equal to the square of the length of the vector P_0P' and PP''. Thus

$$|P_0P'| = ds_0 \ , \ |PP''| = ds \tag{10}$$

and

$$ds_0^2 = dx^i dx^i$$

$$ds^2 = dy^i dy^i \tag{11}$$

where dy^i are evaluated for a fixed time t and are related to dx^j by Eq. (9).

The original propellant is shown in Fig. 14 to be described by general curvilinear coordinates θ_i. Note that in this system θ_i is Lagrangian in character since the system is attached to point P during the deformation process.

$$x_i = x_i(\theta_1, \theta_2, \theta_3) \tag{12}$$

One can easily observe that in the straining process the curvilinear system can be expressed at any instant t by Eq. (12), (13), (14), and (15).

$$y_i = y_i(\theta_1, \theta_2, \theta_3, t) \tag{13}$$

Analogous to Eq. (9)

$$d\theta^i = \frac{\partial \theta^i}{\partial x^j} dx^j \qquad d\theta_i = \frac{\partial x^j}{\partial \theta^i} dx_j$$

$$dx^i = \frac{\partial x^i}{\partial \theta_j} d\theta^j \qquad dx_i = \frac{\partial \theta^j}{\partial x^i} d\theta_j \tag{14}$$

and from Eq. (9)

$$dy^i = \frac{\partial y^i}{\partial \theta^j} d\theta^j \quad , \quad d\theta^i = \frac{\partial \theta^j}{\partial y^i} dy^j \tag{15}$$

It should be noted that $d\theta^i$ remains a contravariant vector under all transformations including transformations of coordinate systems in the deforming process. This is not the case with the covariant vector $d\theta_i$. Thus Eq. (11) is now written in general terms as

$$ds_0^2 = dx^i dx^i = g_{ij} d\theta^i d\theta^j$$

$$ds^2 = dy^i dy^i = G_{ij} d\theta^i d\theta^j \tag{16}$$

where g_{ij} and G_{ij} are the covariant metric tensors of the two states of deformation under investigation. The functions are found for a given time t and are therefore functions of t as well as of $\theta_1, \theta_2, \theta_3$. These functions are mathematically defined as follows:

$$g_{ij} = \frac{\partial x^m}{\partial \theta^i} \frac{\partial x^m}{\partial \theta^j} \quad , \quad g^{ij} = \frac{\partial \theta^i}{\partial x^m} \frac{\partial \theta^j}{\partial x^m} \tag{17}$$

with an example expansion:

$$g_{11} = \frac{\partial x^1}{\partial \theta^1} \frac{\partial x^1}{\partial \theta^1} + \frac{\partial x^2}{\partial \theta^1} \frac{\partial x^2}{\partial \theta^1} + \frac{\partial x^3}{\partial \theta^1} \frac{\partial x^3}{\partial \theta^1}$$

g_{ij} = etc., to give a determinant

$$g = |g_{ij}| = \begin{vmatrix} g_{11} & g_{12} & g_{13} \\ g_{21} & g_{22} & g_{23} \\ g_{31} & g_{32} & g_{33} \end{vmatrix}$$

and

$$G_{ij} = \frac{\partial y^m}{\partial \theta^i} \frac{\partial y^m}{\partial \theta^j}, \quad G^{ij} = \frac{\partial \theta^i}{\partial y^m} \frac{\partial \theta^j}{\partial y^m} \tag{18}$$

with an example expansion:

$$G_{11} = \frac{\partial y^1}{\partial \theta^1} \frac{\partial y^1}{\partial \theta^1} + \frac{\partial y^2}{\partial \theta^1} \frac{\partial y^2}{\partial \theta^1} + \frac{\partial y^3}{\partial \theta^1} \frac{\partial y^3}{\partial \theta^1}$$

CONFIDENTIAL

G_{ij} = etc., to give a determinant

$$G = |G_{ij}| = \begin{vmatrix} G_{11} & G_{12} & G_{13} \\ G_{21} & G_{22} & G_{23} \\ G_{31} & G_{32} & G_{33} \end{vmatrix}$$

We now compare the distance ds_0 at P_0 with ds at P as follows:

$$ds^2 - ds_0^2 = (G_{ij} - g_{ij})\, d\theta^i\, d\theta^j \tag{19}$$

As stated in Eq. (6) the strain tensor is defined as

$$\varepsilon_{ij} = \frac{1}{2}(G_{ij} - g_{ij})$$

Now if a strain measurement experiment is performed that will measure in cartesian coordinates the strains at a point, both before and after deformation, then the magnitude of finite strain is to be computed from

$$\begin{aligned}
\varepsilon_{11} &= \frac{\partial u_1}{\partial x_1} + \frac{1}{2}\left\{\left(\frac{\partial u_1}{\partial x_1}\right)^2 + \left(\frac{\partial u_2}{\partial x_1}\right)^2 + \left(\frac{\partial u_3}{\partial x_1}\right)^2\right\} \\
\varepsilon_{22} &= \frac{\partial u_2}{\partial x_2} + \frac{1}{2}\left\{\left(\frac{\partial u_1}{\partial x_2}\right)^2 + \left(\frac{\partial u_2}{\partial x_2}\right)^2 + \left(\frac{\partial u_3}{\partial x_2}\right)^2\right\} \\
\varepsilon_{33} &= \frac{\partial u_3}{\partial x_3} + \frac{1}{2}\left\{\left(\frac{\partial u_1}{\partial x_3}\right)^2 + \left(\frac{\partial u_2}{\partial x_3}\right)^2 + \left(\frac{\partial u_3}{\partial x_3}\right)^2\right\} \\
\varepsilon_{12} &= \frac{1}{2}\left(\frac{\partial u_1}{\partial x_2} + \frac{\partial u_2}{\partial x_1}\right) + \frac{1}{2}\left(\frac{\partial u_1}{\partial x_1}\frac{\partial u_1}{\partial x_2} + \frac{\partial u_2}{\partial x_1}\frac{\partial u_2}{\partial x_2} + \frac{\partial u_3}{\partial x_1}\frac{\partial u_3}{\partial x_2}\right) \\
\varepsilon_{23} &= \frac{1}{2}\left(\frac{\partial u_2}{\partial x_3} + \frac{\partial u_3}{\partial x_2}\right) + \frac{1}{2}\left(\frac{\partial u_1}{\partial x_2}\frac{\partial u_1}{\partial x_3} + \frac{\partial u_2}{\partial x_2}\frac{\partial u_2}{\partial x_3} + \frac{\partial u_3}{\partial x_2}\frac{\partial u_3}{\partial x_3}\right) \\
\varepsilon_{13} &= \frac{1}{2}\left(\frac{\partial u_1}{\partial x_3} + \frac{\partial u_3}{\partial x_1}\right) + \frac{1}{2}\left(\frac{\partial u_1}{\partial x_1}\frac{\partial u_1}{\partial x_3} + \frac{\partial u_2}{\partial x_1}\frac{\partial u_2}{\partial x_3} + \frac{\partial u_3}{\partial x_1}\frac{\partial u_3}{\partial x_3}\right)
\end{aligned} \tag{20}$$

where

x_1, x_2, x_3 = undeformed cartesian base frame

u_1, u_2, u_3 = corresponding displacements with respect to x_1, x_2, x_3.

Note that Eq. (7) may be obtained by neglecting the shear terms in Eq. (20).

5. Point Strains Versus Structural Strains

The mathematics presented above describes point strain phenomena. Experiments performed in a laboratory are usually concerned with the over-all displacements of a structure. Regardless of the over-all dimensions of a specimen, it is usually loaded as a structure. That is to say, simple loadings are difficult to apply. Usually the experimentalist neglects the boundary strains due to bending, shear, and torsion by the St. Venant Principle. It is a common practice to assume that structurally determined strains are equivalent to intrinsic point strains because of expediency. In practice there is a tendency to confuse structural analysis with basic point analysis. Whereas, to proceed from basic point analysis to structural analysis is correct, the converse is not necessarily true. An obvious example is that of a deformed beam. Here the strain can be computed knowing the stress at a point using basic point analysis. However, the stress determination at the point is determined from geometric considerations prevalent to structural analysis.

A more pertinent example is illustrated by biaxially pressurizing an unrestricted propellant grain. Here an over-all longitudinal contraction might experimentally be expected. Nevertheless an unusual barreling structural deformation occurs with a consequential end effect (Fig. 11). To indicate that the over-all longitudinal contraction measures an average point strain is analogous to assuming that a cube deforms into a rhombohedron instead of a curvilinear parallelepiped in a shear experiment.

In summary it is noted that a line constructed of points in or on an undeformed body (structure) will usually become skew upon deformation of the body. Consequently, if a cartesian coordinate system is chosen for the curvilinear system θ^i in the undeformed state, it will in general be difficult to express the structural boundary conditions because the structure will be transformed into a natural curvilinear system ψ^i. Thus, except for specific experiments such as described by Rivlin (Ref. 27), the mathematical concepts of strain presented above become unwieldy for practical experimental applications. However, if experimentally the principal strains can be measured in the close proximity of a point both before and after loading, this transformation difficulty is overcome from a practical (engineering) point of view. This is because at a point origin, the curvilinear strains in the deformed state approach in magnitude the cartesian strain (Fig. 13). It is for this reason that the photoelastic coating technique was developed for the study of propellant physical properties. No matter what contortions the over-all structure experiences, the photoelastic coating technique will only measure the biaxial principal strains at a point region on the structure.

CONFIDENTIAL

CONFIDENTIAL

6. Strain Invariants

Utility of Eq. (1) is predicated on the usage of the proper strain invariants I_1, I_2, and I_3. A mathematical definition of the invariants is as follows:

$$I_1 = g^{rs}G_{rs} \;;\; I_2 = G^{rs}g_{rs}I_3 \;;\; I_3 = \frac{G}{g} \qquad (21)$$

A geometric description is evidently not obvious from Eq. (21). However, if one needed a schematic model to visualize these invariants, perhaps the notion of a particular set of three skew fibers that remained skew (invariant) under deformations may suffice. In Ref. 28, a good physical interpretation of strains is presented. Perhaps further study of this reference can lead to a better geometric notion of strain invariants.

Emphasis should be made that the strain invariants I_1, I_2, and I_3 must be derived for any particular class of deformation in accord with Eq. (21). In essence the general practice is to choose a structure and assume its strain state (note that this is quite complicated except for a point analysis).

The form of the invariants (I_1, I_2, and I_3) listed in Eq. (1) is only applicable to describe the straining of a cube into a cuboid. It is obvious that only cartesian coordinates would be considered to represent the material and spacial (Ref. 29) reference frames for this particular geometric deformation. Should a different kind of deformation be considered, then another description of the invariants would be in order (Ref. 26). Another advantage in using cartesian coordinates is that no distinction need arise between covariant and contravariant differentiation. Thus, the use of cartesian coordinates in the theory suggests that the three principal strains be experimentally measured in cartesian coordinates. Eq. (22) is obtained by differentiating the invariants defined in Eq. (1).

The magnitudes of these invariant gradients at a point may then be computed knowing the principal strains ($\varepsilon_1 = \varepsilon_{11}$, $\varepsilon_2 = \varepsilon_{22}$, $\varepsilon_3 = \varepsilon_{33}$):

$$\frac{\partial I_1}{\partial \varepsilon_1} = 2 + 2\varepsilon_1 \qquad \frac{\partial I_1}{\partial \varepsilon_2} = 2 + 2\varepsilon_2 \qquad \frac{\partial I_1}{\partial \varepsilon_3} = 2 + 2\varepsilon_3$$

$$\frac{\partial I_2}{\partial \varepsilon_1} = 4 + 4\varepsilon_1 + 4\varepsilon_2 + 4\varepsilon_3 + 2\varepsilon_1\varepsilon_2^2 + 2\varepsilon_1\varepsilon_3^2 + 4\varepsilon_1\varepsilon_2 + 4\varepsilon_3\varepsilon_1 + 2\varepsilon_2^2 + 2\varepsilon_3^2$$

$$\frac{\partial I_2}{\partial \varepsilon_2} = 4 + 4\varepsilon_1 + 4\varepsilon_2 + 4\varepsilon_3 + 4\varepsilon_1\varepsilon_2 + 4\varepsilon_2\varepsilon_3 + 2\varepsilon_1^2\varepsilon_2 + 2\varepsilon_2\varepsilon_3^2 + 2\varepsilon_1^2 + 2\varepsilon_3^2$$

$$\frac{\partial I_2}{\partial \varepsilon_3} = 4 + 4\varepsilon_1 + 4\varepsilon_2 + 4\varepsilon_3 + 4\varepsilon_2\varepsilon_3 + 4\varepsilon_1\varepsilon_3 + 2\varepsilon_3\varepsilon_2^2 + 2\varepsilon_1^2\varepsilon_3 + 2\varepsilon_2^2 + 2\varepsilon_1^2$$

$$\frac{\partial I_3}{\partial \varepsilon_1} = 2 + 4\varepsilon_2 + 2\varepsilon_2^2 + 2\varepsilon_1 + 4\varepsilon_2\varepsilon_1 + 2\varepsilon_1\varepsilon_2^2 + 4\varepsilon_3 + 8\varepsilon_2\varepsilon_3 + 4\varepsilon_3\varepsilon_2^2 + 4\varepsilon_1\varepsilon_3 + 8\varepsilon_2\varepsilon_3\varepsilon_1 + 4\varepsilon_1\varepsilon_3\varepsilon_2^2 + 2\varepsilon_3^2 + 4\varepsilon_2\varepsilon_3^2 + 2\varepsilon_2^2\varepsilon_3^2 + 2\varepsilon_1\varepsilon_3^2 + 4\varepsilon_2\varepsilon_1\varepsilon_3^2 + 2\varepsilon_1\varepsilon_2^2\varepsilon_3^2 \qquad (22)$$

$$\frac{\partial I_3}{\partial \varepsilon_2} = 2 + 2\varepsilon_2 + 4\varepsilon_1 + 4\varepsilon_1\varepsilon_2 + 2\varepsilon_1^2 + 2\varepsilon_1^2\varepsilon_2 + 4\varepsilon_3 + 4\varepsilon_2\varepsilon_3 + 8\varepsilon_1\varepsilon_3 + 8\varepsilon_1\varepsilon_3\varepsilon_2 + 4\varepsilon_3\varepsilon_1^2 + 4\varepsilon_2\varepsilon_3\varepsilon_1^2 + 2\varepsilon_3^2 + 2\varepsilon_2\varepsilon_3^2 + 4\varepsilon_1\varepsilon_3^2 + 4\varepsilon_1\varepsilon_2\varepsilon_3^2 + 2\varepsilon_1^2\varepsilon_3^2 + 2\varepsilon_1^2\varepsilon_2\varepsilon_3^2$$

$$\frac{\partial I_3}{\partial \varepsilon_3} = 2 + 4\varepsilon_2 + 2\varepsilon_2^2 + 4\varepsilon_1 + 8\varepsilon_1\varepsilon_2 + 4\varepsilon_1\varepsilon_2^2 + 2\varepsilon_1^2 + 4\varepsilon_2\varepsilon_1^2 + 2\varepsilon_1^2\varepsilon_2^2 + 2\varepsilon_3 + 4\varepsilon_2\varepsilon_3 + 2\varepsilon_3\varepsilon_2^2 + 4\varepsilon_1\varepsilon_3 + 8\varepsilon_1\varepsilon_2\varepsilon_3 + 4\varepsilon_1\varepsilon_3\varepsilon_2^2 + 2\varepsilon_1^2\varepsilon_3 + 4\varepsilon_2\varepsilon_3\varepsilon_1^2 + 2\varepsilon_1^2\varepsilon_2^2\varepsilon_3$$

Consider the mathematical simplifications introduced by using point cartesian strain invariants and restrict the investigation to orthogonal coordinates, where the three families of coordinate surfaces are mutually perpendicular. If the experimental measurements are made at a point in cartesian coordinates, then an approximation can be made of the magnitudes associated with an appropriate curvilinear coordinate frame at that point. Integration from point to point using analytical theory in curvilinear coordinates would then yield the stress-strain response of the structure being studied. It is evident that the only reason a curvilinear system is chosen at some point in space is because it is simpler to express the boundary conditions of the vector field in natural coordinates. There is no reason to generalize the use of a curvilinear coordinate system for structure of arbitrary shape, e.g., a propellant cylinder.

7. A Proposed Analytical Description of the Strain Energy Function W

The strain energy function W, as its name would imply, is the amount of recoverable energy (in.-lb/in.^{3} = psi) stored in a deformed volume. From a mathematical point of view, W may be considered as an analog equivalent of the Lamé constants in linear elastic theory.

Prior to attempting to characterize W, the magnitudes of Ю, И and Я in Eq. (3) must be obtained. Since the

CONFIDENTIAL

point principal stresses are available using Eq. (4), Eq. (3) may be rewritten for a homogeneous deformation in terms of the principal cartesian strains as

$$\tau_{11} = \frac{1}{\sqrt{I_3}}\left\{Ю\frac{\partial I_1}{\partial \varepsilon_{11}} + И\frac{\partial I_2}{\partial \varepsilon_{11}} + Я\frac{\partial I_3}{\partial \varepsilon_{11}}\right\}$$

$$\tau_{22} = \frac{1}{\sqrt{I_3}}\left\{Ю\frac{\partial I_1}{\partial \varepsilon_{22}} + И\frac{\partial I_2}{\partial \varepsilon_{22}} + Я\frac{\partial I_3}{\partial \varepsilon_{22}}\right\} \qquad (23)$$

$$0 = \frac{1}{\sqrt{I_3}}\left\{Ю\frac{\partial I_1}{\partial \varepsilon_{33}} + И\frac{\partial I_2}{\partial \varepsilon_{33}} + Я\frac{\partial I_3}{\partial \varepsilon_{33}}\right\}$$

If at a point ε_{11}, ε_{22}, ε_{33} are measured explicitly so that the invariant gradients can be calculated, and τ_{11}, τ_{22} are calculated from the pressure and the cylindrical dimensions according to Eq. (4) then these data can be utilized in Eq. (23) to solve for Ю, И, Я.

The proper mathematical characterization of W is subjective. The simplest characterization would be to expand $W(I_1, I_2, I_3)$ in a Taylor series about $I_1 = 3$, $I_2 = 3$, $I_3 = 1$, for $W = 0$, and arbitrarily neglect higher order derivatives. The functional form would then be somewhat more general than existing proposed forms[3]:

$$W = Ю(I_1 - 3) + И(I_2 - 3) + Я(I_3 - 1) \qquad (24)$$

The mode of W versus I_1, W versus I_2 and W versus I_3 should indicate what the functional form of W could be for any specific propellant. Experimentally, therefore, the problem of finding W is reduced to one of finding the three principal strains at a point on the surface of a cylinder.

8. Computer Solutions of Photoelastic Coating Strains

Since the immediate interest concerns tubular unrestricted propellant grains, the graphical separation of the principal stresses measured in the bonded photoelastic coatings at various points have been programmed. In previous reports (*QSR* 38-3 through 38-9) a graphical technique was utilized. This same technique is the basis of the computer solution. Having established that the plane stress condition exists in a photoelastic coating, the principal stresses are separated as follows. The resulting shear stress σ_ψ at a point in a general two-dimensional stress system may be expressed as

$$\sigma_\psi = \frac{\sigma_{11} - \sigma_{22}}{2}\sin 2\psi - \sigma_{12}\cos 2\psi \qquad (25)$$

where ψ is the angle of rotation about a point with respect to the normal stress in the coating.

In retrospect it is noted that there is no shear along any radial trace for a pressurized cylinder because of symmetry. Therefore, Eq. (25) reduces to

$$\sigma_\psi = \frac{\sigma_{11} - \sigma_{22}}{2}\sin 2\psi \qquad (26)$$

for any point along a radial trace. Next, n equally spaced inspection points on the coating along one radial trace are selected. About these inspection points a plane element dr, $rd\theta$, is designated. In the limit this element approaches dx, dy (Fig. 13). By arbitrarily choosing $\psi = 1$ deg, Eq. (26) can be applied at the edge of the element to obtain a shear parallel to the radius $\theta = 90$ deg (Fig. 13). Thus with respect to a point i in the cartesian system, Eq. (26) becomes

$$\overset{i}{\sigma}_{xy} = 0.01745\,[\sigma_{11} - \sigma_{22}]_i \qquad (27)$$

The magnitude of $[\sigma_{11} - \sigma_{22}]_i$ is obtained directly from the previously calibrated isochromatic spectrum that corresponds to the point i under investigation.

It is necessary to reference the shear stress $\overset{i}{\sigma}_{xy}$ with respect to the axis of the cylinder. In this manner the fringe value of the isochromatic trace (in psi) can be directly assigned to Eq. (27), since the trace is originally measured with reference to the cylinder axis. In cartesian coordinates the distance x from a point on the reference radius ($\theta = 90$ deg) to the shear stress σ_{xy} may be expressed as

$$x_i = 0.01746\,[y_n + \delta(n - i)] \qquad (28)$$

where

y_i = radial distance to point

y_n = innermost point (its magnitude is equal to the number of points under investigation)

δ = equal increment $(y_1 - y_n)/(n - 1)$

[3]It is noted that by including the higher order derivatives and factoring the invariants, generalization of Ю, И, and Я as functions of I_1, I_2, and I_3 is possible.

CONFIDENTIAL

In the close proximity of the point under investigation (noting that $\overset{i}{\sigma}_{xy} = 0$ at $x_i = 0$) the shear $\overset{i}{\sigma}_{xy}$ with respect to x_i may be approximated in incremental form

$$\frac{\Delta \overset{i}{\sigma}_{xy}}{\Delta x_i} \approx \frac{d\overset{i}{\sigma}_{xy}}{dx_i} \tag{29}$$

From the two-dimensional equilibrium equation it is noted that

$$\frac{\partial \overset{i}{\sigma}_{yy}}{\partial y_i} = -\frac{\partial \overset{i}{\sigma}_{xy}}{\partial x_i} \tag{30}$$

so that the desired quantities $\partial \overset{i}{\sigma}_{yy}/\partial y_i$ are obtained.

The relationship between $\overset{i}{\sigma}_{yy}$ and y_i can be obtained on a computer using Simpson's rule, knowing the boundary conditions $\overset{i}{\sigma}_{yy} = 0$ at y_1. Separation of the principal stresses from isochromatic data is thus achieved knowing the calibrated stress-strain relationship of the linear coating.

The principal strains in the coating are then computed from

$$\begin{aligned} \overset{i}{\varepsilon}_{11} &= \left[\frac{\sigma_{11}}{E} - \frac{\mu}{E}\sigma_{22}\right]_i \\ \overset{i}{\varepsilon}_{22} &= \left[\frac{\sigma_{22}}{E} - \frac{\mu}{E}\sigma_{11}\right]_i \end{aligned} \tag{31}$$

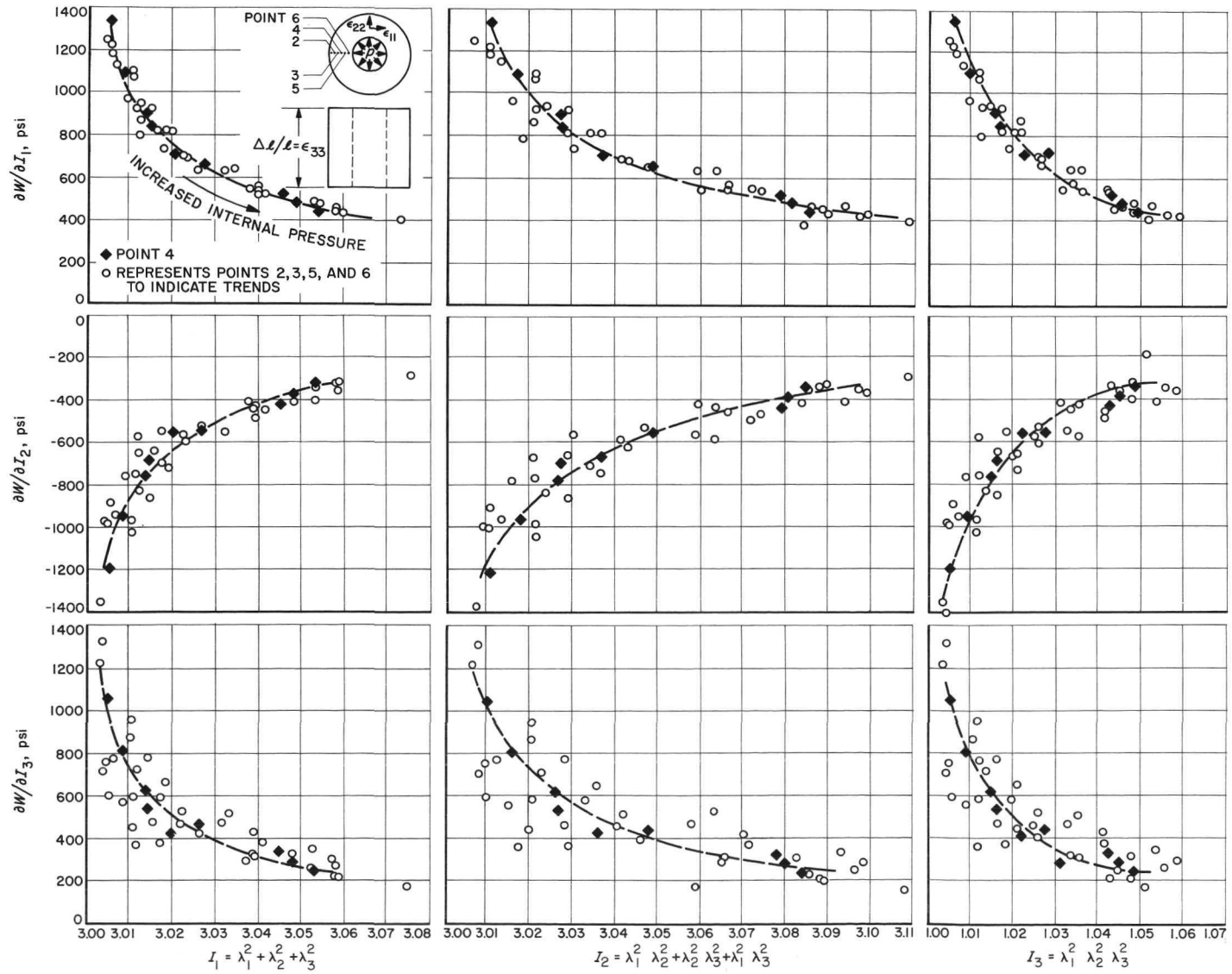

Fig. 16. Potential gradients versus the three invariants at points under varying stresses

CONFIDENTIAL

CONFIDENTIAL

From Eq. (31) the magnitudes of the principal strains ε_{11} and ε_{22} can be obtained and stored in the computer's memory to be used later to compute the invariant gradients Eq. (22).

9. Measurement of Longitudinal Structural Strain

The discrepancy between ideal and actual structural deformation is exaggeratedly shown in Fig. 11. Attention is brought to the difficulties encountered with the measurement of a point longitudinal strain. An extensometer capable of examining the end effect was used to measure a structural strain. The applicability of this strain to the theory is questionable. However, it was found that the magnitude of this longitudinal principal strain was small compared to the biaxial principal strains. Thus, it is presumed that no appreciable error was introduced in this instance because of the use of a structural strain instead of a point strain. The longitudinal extensometer is illustrated in Fig. 12. The reflective polariscope and loading fixture are described in *QSR 38-9*.

10. The Strain Energy Function

The structural strain ε_{33} was only measured at Point 4 (Fig. 16) (center of the coating). Its numerical value was arbitrarily assigned to the other points for strain energy computations, i.e., as though there had been a uniform change in length. Fig. 11 denotes that this assignment is not precise because of the end effect of the cylinder. Biaxial strain data ε_{11} and ε_{22} obtained at Points 2 and 6 are also questionable because of their proximity to the coating edge and also because of cylinder end curvature. Therefore, only Point 4 is considered accurate. The other points are presented only as indicators of trends.

The potential gradients Ю, И, and Я, computed from Eq. (23), are plotted with respect to the invariants I_1, I_2, and I_3 in Fig. 16. A gradient-invariant relationship is shown for Points 2 through 6. A similar mode is observed for each of the nine relationships between the gradients and invariants.

The strain energy function W was assumed to be defined by Eq. (24). Figure 17 illustrates the values (subject to the limitations stated above) of W at the various points for the different stress-strain environments. As one would expect, the strain energy increases with effective strain. At Point 4 the three-dimensional strain energy approaches

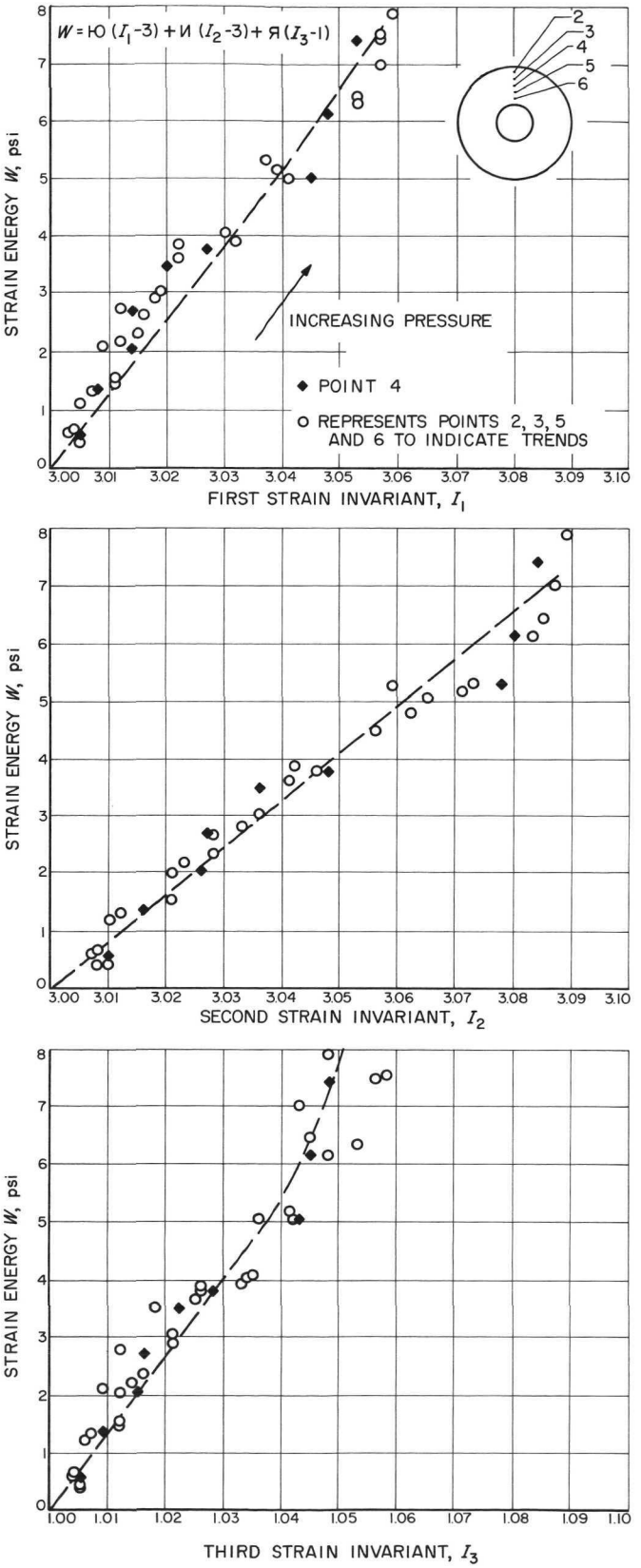

Fig. 17. Strain energy versus the three invariants at points under varying stresses

CONFIDENTIAL

CONFIDENTIAL

7.4 psi for a strain field $\varepsilon_{11} = 0.089$, $\varepsilon_{22} = -0.052$, $\varepsilon_{33} = -0.016$, and a stress field $\tau_{11} = 76.1$ psi, $\tau_{22} = -15.4$ psi, $\tau_{33} = 0$.

It is noted that no control over the invariants could be made with this experiment. Only the internal pressure in the cylinder could be varied. The measured strain state at any arbitrary point on the cylinder depends only on the applied stresses at that point. The strain response of the medium to these stresses determines the potential gradients at the point. The variation of the gradients from point to point, therefore, arises from variation between the individual principal strains. The most significant variance, obviously, was between the radial and circumferential strains in the radial direction.

Finally, the question as to the credibility of the value obtained for the three-dimensional strain energy Eq. (24) can be answered by comparison with uniaxial tensile data. Such data was obtained from a tensile bar cast from the same mix batch. Uniaxial strain energy is defined as

$$W_u = \int_0^{\varepsilon_{11}} \tau_{11}\, d\varepsilon_{11} \tag{32}$$

The magnitude of W (uniaxial) is obtained from the area under the stress-strain curve (neglecting losses). For $\varepsilon_{11} = 0.06, W = 2.8$ psi; $\varepsilon_{11} = 0.08, W = 4.6$ psi; $\varepsilon_{11} = 0.10$, $W = 6.7$ psi. Thus, it is demonstrated that the value obtained for the three-dimensional strain energy is reasonable for Point 4.

11. Summary

An experimental method to determine the strain energy function W in three dimensions for solid propellant has been presented. No assumptions regarding the propellant's physical properties are necessary to obtain the new nonlinear physical property W. The strain energy function for a polyurethane propellant appears to be characterized by

$$W = \text{Ю}\,(I_1 - 3) + \text{И}\,(I_2 - 3) + \text{Я}\,(I_3 - 1)$$

where Ю, И, and Я are the leading partial derivatives in a Taylor expansion of $W(I_1 I_2 I_3)$ about the point $I_1 = 3$, $I_2 = 3$, $I_3 = 1$, for $W = 0$. Conventional uniaxial experimental data independently confirms the order of magnitude of the strain energy function obtained from the above equation.

References

1. Moacanin, J., "Diisocyanate-Linked Polymers. I. Dilute Solution Properties of Toluene Diisocyanate-Extended Polypropylene Glycol," *Journal of Applied Polymer Science*, Vol. 1, pp. 272–282, 1959.
2. Grassie, N., *Chemistry of High Polymer Degradation Processes*, Butterworths Publications, London, 1956.
3. Treloar, L. R. G., *The Physics of Rubber Elasticity*, p. 85, Oxford University Press, New York, N. Y., 1958.
4. Flory, P. J., "Theory of Elastic Mechanisms in Fibrous Proteins," *Journal of the American Chemical Society*, Vol. 78, p. 5222, 1956.
5. Flory, P. J., and Daoust, H., "Osmotic Pressures of Moderately Concentrated Polymer Solutions," *Journal of Polymer Science*, Vol. 25, p. 429, 1957.
6. Orofino, T. A., and Flory, P. J., "Relationship of the Second Virial Coefficient to Polymer Chain Dimensions and the Interaction Parameters," *Journal of Chemical Physics*, Vol. 26, p. 1067, 1957.
7. Smith, T. L., "Dependence of the Ultimate Properties of a SBR Rubber on Strain Rate and Temperature," *Journal of Polymer Science*, Vol. 32, p. 99, 1958.

CONFIDENTIAL

References (Cont'd)

8. Smith, T. L., "Volume Change and Dewetting in Glass Bead-Polyvinyl Chloride Composites Under Large Deformation," *Transactions of the Society of Rheology,* Vol. 3, p. 113, 1959.

9. Hwa, J. C. H., "Measurements on the Degree of Cross-linking of High-Conversion Post-Gelation Methyl Methacrylate–Methylene Dimethacrylate Copolymers," *Journal of Polymer Science,* Vol. 58, p. 715, 1962.

10. Hewitt, F. G., and Anthony, R. L., "Measurement of the Isothermal Volume Dilation Accompanying the Unilateral Extension of Rubber," *Journal of Applied Physics,* Vol. 29, p. 1411, 1958.

11. Mullins, L., and Tobin, N. R., "Carbon-Black Loaded Rubber Vulcanizates: Volume Changes in Stretching," *Transactions of the Institute of Rubber Industries,* Vol. 33, p. 2, 1957.

12. Kusov, A. B., Trofimova, V. I., and Nilova, Yu. I., "Changes in the Specific Volume of Rubber During Elongation," *Rubber Chemistry and Technology,* Vol. 31, p. 513, 1958.

13. Becker, G. W., and Vogel, K., "Spannungerelaxation von Hochpolymeren bei verschiedenen Beanspruchungsarten," *Zeitschrift für Elektrochemie,* Vol. 65, pp. 696–699, 1961.

14. San Miguel, A., "An Experimental Method to Measure the Strain Energy Function *W*," Technical Report 32-365, Jet Propulsion Laboratory, California Institute of Technology, Pasadena, December 20, 1962.

15. "Study of Mechanical Properties of Solid Rocket Propellants," Aerojet General Corp., Sacramento, Calif., Report No. 0411-10F, March 1962, p. 109.

16. "Fracture Mechanics of Solid Propellants," E. I. duPont de Nemours and Co., Eastern Laboratory, Gibbstown, N. J., Report ELab-A-31, February 15, 1961, p. 9.

17. Blatz, P. J., and Ko, W. L., "Application of Finite Elastic Theory to the Deformation of Rubbery Materials," *Transactions of the Society of Rheology,* Vol. VI, pp. 223–251, 1962.

18. "Study of Mechanical Properties of Solid Rocket Propellants," Aerojet General Corp., Sacramento, Calif., Report No. 0411-10F, March 1962, p. 26.

19. Ignatowski, A. J., "Review of Multiaxial Testing of Propellant," 20th JANAF Meeting Addendum, John Hopkins University, Silver Springs, Md., November 14–16, 1961, p. 1.

20. "The Viscoelastic Behavior of Composite Solid Propellant," Thiokol Chemical Corp., Report No. 8-62, April 22, 1962, Redstone Division, Huntsville, Ala., p. 45.

21. "Study of Mechanical Properties of Solid Rocket Propellants," Aerojet General Corp., Sacramento, Calif., Report No. 0411-10F, March 1962, p. 67.

22. Reiner, M., "Deformation, Strain and Flow," Interscience Publishers, Inc., New York, N. Y., 1960.

23. Truesdell, C., and Toupin, R., "The Classical Field Theories," Handbuck Der Physik, S. Flugge, Editor, Volume III/1, Springer-Verlag, Berlin, 1960, pp. 226–793.

References (Cont'd)

24. Sneddon, I. N., and Berry, D. S., "The Classical Theory of Elasticity," Handbuch Der Physik, Volume VI, S. Flugge, Editor, Springer-Verlag, Berlin, 1958, Vol. 17, p. 3.

25. Rivlin, R. S., "A Series of Eight Lectures on Finite Elastic Deformations," California Institute of Technology, Pasadena, January–February, 1953.

26. Green, A. E., and Zerna, W., *Theoretical Elasticity*, Oxford University Press, New York, N. Y., 1960.

27. Rivlin, R. S., *Philosophical Transactions of the Royal Society of London*, Vol. A240, 1948, pp. 459, 491, 509; Vol. A241, 1949, p. 379; Vol. A242, 1950, p. 173; Vol. A243, 1951, p. 251; and *Proceedings of the Royal Society of London*, Vol. A195, 1949, p. 463.

28. Novozhilov, V. V., *Foundations on the Nonlinear Theory of Elasticity*, Graylock Press, Rochester, N. Y., 1953.

29. Prager, W., *Introduction to Mechanics of Continua*, p. 62, Ginn and Co., N. Y., 1961.

CONFIDENTIAL

UNCLASSIFIED

This document contains information affecting the national defense of the United States, within the meaning of the Espionage Laws, Title 18, U.S.C., Sections 793 and 794, the transmission or revelation of which in any manner to an unauthorized person is prohibited by law.

CONFIDENTIAL